

HNF-4769, Rev. 1

FAR-FIELD HYDROLOGY DATA PACKAGE

FOR

**IMMOBILIZED LOW-ACTIVITY TANK WASTE
PERFORMANCE ASSESSMENT**

Raz Khaleel
Fluor Daniel Northwest, Inc.
P.O. Box 1050
Richland, WA 99352

December, 1999

EXECUTIVE SUMMARY

A number of data packages are being assembled as part of 2001 Immobilized Low-Activity Tank Waste (ILAW) Performance Assessment (PA). This data package deals with the far-field hydrology data needed to perform vadose zone flow and transport modeling for the ILAW PA.

The ILAW PA shall be conducted for two sites; the new ILAW disposal site and the existing disposal site east of the new ILAW site in 200 East Area. Site characterization data are available for both sites. This report presents the laboratory measurements on physical and hydraulic properties for soil samples at the disposal sites, and results on application of stochastic theory to small-scale measurements. The effective (upscaled) parameter estimates are derived for saturated hydraulic conductivity, soil moisture retention and unsaturated hydraulic conductivity, bulk density, unretarded macrodispersivity and sorption-enhanced macrodispersivity. These parameters will serve as input to VAM3DF, a variably saturated vadose zone flow and transport code; VAM3DF will generate 'mean' solutions for the pressure head and contaminant concentration.

The stratigraphy at both disposal sites is dominated by two distinctly different sediment sequences. The upper part of the vadose zone is characterized by a sandy sequence, whereas the lower part is characterized primarily by a gravel sequence. At saturation, compared to the gravel-dominated sequence, the sand-dominated sequence is described by a smaller log-conductivity variance. However, compared to the gravel-dominated sequence, the log-unsaturated conductivity variance for the sand-dominated sequence is higher. Consequently, the macroscopic anisotropy relations for the sandy and gravelly sediments are different. The differences in the characteristics of the two sediment sequences also result in different macrodispersivity estimates. Overall, compared to sandy soils, gravelly soils are characterized by a much smaller saturated water content, higher bulk density, higher log-conductivity variance, smaller log-unsaturated conductivity variance, a much smaller macroscopic anisotropy and smaller macrodispersivities.

A methodology is presented to estimate uncertainties in model predictions. For far-field hydrology, three sources contribute to uncertainty estimates: (a) variations in model configurations, (b) uncertainties in the calculated mean solution for concentration, and (c) uncertainties around the calculated mean solution for concentration. The following approach will be used to evaluate these uncertainties. First, uncertainty will be defined for the 'mean' solutions for concentration distribution at the water table (as a function of position and time). The combined contribution to uncertainty in the mean solution due to model configuration and effective parameter (i.e., unsaturated hydraulic conductivity and macrodispersivity) variations will be investigated. A methodology developed by Kapoor and Gelhar (1994a,b) will then be used to estimate the uncertainty around the mean solution.

Model configurations will include variations in stratigraphy and clastic dike networks. Base case and uncertainty in stratigraphy and clastic dike network models will be provided in the geology data package. Selected VAM3DF runs will be performed to estimate the impact of these uncertainties on the resultant contaminant distribution at the water table. The uncertainty attributed to isotropy and sloped layering on calculated mean solutions will also be estimated.

Bounding estimates for concentrations at the water table will be provided through a choice of parameters and model configurations judged to provide a worst case representation of the system.

CONTENTS

1.0 Introduction 1

 1.1 SCOPE OF THIS DATA PACKAGE 1

2.0 Laboratory Measurements for Soil Physical and Hydraulic Properties 4

 2.1 NEW ILAW DISPOSAL SITE 4

 2.1.1 100 Area Samples 5

 2.2 EXISTING DISPOSAL SITE 9

3.0 Effective (Upscaled) Flow and Transport Properties 13

 3.1 EFFECTIVE (UPSCALED) FLOW PARAMETERS 13

 3.1.1 Stochastic Upscaling 14

 3.1.2 Field Observations 14

 3.1.3 Composite Macroscopic Relationships 14

 3.1.3.1 Stochastic Model for Macroscopic Anisotropy 15

 3.1.3.2 Macroscopic Anisotropy Relations 18

 3.2 EFFECTIVE TRANSPORT PARAMETERS 20

 3.2.1 Bulk Density 21

 3.2.2 Diffusivity 21

 3.2.3 Dispersivity 22

 3.2.3.1 Saturated Media Dispersivities For Field Sites 22

 3.2.3.2 Vadose Zone Dispersivities For Dry Desert Environment 24

 3.2.3.3 Stochastic Models and Macrodispersivities for Large-Scale Media 25

 3.2.3.4 Macrodispersivity Estimates For Non-Reactive Species 26

 3.2.3.5 Heterogeneous Sorption Enhanced Macrodispersivities 27

 3.2.3.6 Numerical Considerations 30

4.0 Uncertainties in Model Predictions 35

 4.1 MODEL CONFIGURATIONS 35

 4.1.1 Variations in Stratigraphy 35

 4.1.2 Clastic dikes 36

 4.1.3 Isotropy 38

 4.1.4 Sloped Layering 38

 4.2 UNCERTAINTIES IN THE MEAN SOLUTION DUE TO VARIATIONS OF EFFECTIVE PARAMETER ESTIMATES 38

 4.3 UNCERTAINTIES AROUND THE MEAN SOLUTION 39

 4.4 BOUNDING ESTIMATES 39

5.0 REFERENCES 41

6.0 PEER REVIEW 46

LIST OF TABLES

Table 1. Van Genuchten parameters (based on the multistep method), saturated hydraulic conductivity, and bulk density data for 20 ILAW borehole samples from the sandy sequence (after Fayer et al. 1998). 6

Table 2. Van Genuchten parameters, fitted saturated hydraulic conductivity, and measured bulk density data for 15 sandy gravel samples..... 8

Table 3. Comparison of mean parameter estimates for the sandy sequence at the new ILAW and existing disposal sites..... 9

Table 4. Composite van Genuchten-Mualem parameters for the sand- and gravel-dominated sequences..... 15

Table 5. Macroscopic anisotropy parameters for the sand- and gravel-dominated sequences. ... 19

Table 6. Effective parameter estimates, $E[\bullet_b K_d]$, for the product of bulk density (g/cm^3) and K_d (cm^3/g) at the new ILAW and existing disposal sites. 21

Table 7. Non-reactive macrodispersivity estimates for soils at the new ILAW and existing disposal sites..... 27

Table 8. Macrodispersivity enhancement for the sandy sequence at the new ILAW and existing disposal sites [\bullet_b in g/cm^3 and K_d in cm^3/g]..... 29

Table 9. Macrodispersivity enhancement for the gravelly sequence at the new ILAW and existing disposal sites [\bullet_b in g/cm^3 and K_d in cm^3/g]..... 30

Table 10. Van Genuchten parameters (based on the multistep method), saturated hydraulic conductivity, and bulk density for seven clastic dike samples (after Fayer and Ritter 1999)..... 37

LIST OF FIGURES

Figure 1. Modeling strategy for assessing ILAW disposal system impacts (after McGrail et al. 1998)..... 2

Figure 2. Geologic cross section of the new ILAW disposal site (after Reidel et al. 1998). 7

Figure 3. Particle-size distribution for 20 samples from the sand-dominated sequence at the new ILAW disposal site..... 8

Figure 4. Fitted moisture retention and unsaturated conductivity curves for 20 samples for the sand-dominated sequence (the symbols represent various samples, not experimental data). 10

Figure 5. Fitted moisture retention and unsaturated conductivity curves for 15 samples for the gravel-dominated sequence (the symbols represent various samples, not experimental data). 11

Figure 6. Geologic cross section of the existing disposal site (after Kincaid et al. 1995). 12

Figure 7. Composite moisture retention and unsaturated conductivity curves for the sand-dominated sequence. 17

Figure 8. Composite moisture retention and unsaturated conductivity curves for the gravel-dominated sequence. 18

Figure 9. Experimental (triangles) and fitted theoretical (squares) variogram for LnKs..... 19

Figure 10. Calculated macroscopic anisotropy (equation 3) as a function of mean pressure head for the sand-dominated sequence. 20

Figure 11. Calculated macroscopic anisotropy (equation 3) as a function of mean pressure head for the gravel-dominated sequence. 20

Figure 12. Longitudinal macrodispersivity in saturated media as a function of overall problem scale with data classified by reliability (after Gelhar et al. 1992)..... 23

Figure 13. Longitudinal macrodispersivity in unsaturated media as a function of overall problem scale (after Gelhar 1993). [Note that the triangles are data from Ward et al. 1998]..... 24

Figure 14. LnK versus R for (a) Cs-137, (b) Sr-90, (c) U, and (d) Se for the sand-dominated sequence. 32

Figure 15. LnK versus R for (a) Cs-137, (b) Sr-90, (c) U, and (d) Se for the gravel-dominated sequence. 34

Figure 16. Schematic of concentration (C) distribution at the water table. 36

APPENDICES

Appendix A. Physical and Hydraulic Measurements of FY1998 Borehole Cores A-i

Appendix B. Laboratory Data on Physical and Hydraulic Properties for 100 Area Samples (RETC Input File) B-i

Appendix C. Hydraulic Parameters of the Upper Hanford Formation C-i

Appendix D. Physical and Hydraulic Measurements of FY1998 Clastic Dike Samples..... D-i

Appendix E. Quality Assurance/Quality Control (QA/QC) Considerations..... E-i

1.0 INTRODUCTION

The *Hanford Immobilized Low-Activity Tank Waste Performance Assessment* examines the long-term environmental and human health effects associated with the planned disposal of the vitrified low-level fraction of the waste presently contained in Hanford Site High-Level Waste Tanks. The objectives of the performance assessment are to provide a reasonable expectation that the disposal of the waste will be protective of the general public, groundwater resources, air resources, inadvertent intruder and surface water resources. A number of data packages are being assembled as part of 2001 Immobilized Low-Activity Tank Waste (ILAW) Performance Assessment (PA). This data package deals only with the far-field (Figure 1) hydrology data needed to perform vadose zone flow and transport modeling for the ILAW PA.

Figure 1 illustrates also the overall computational strategy for the ILAW PA. The near-field environment is defined as the domain through the vault to some distance below the floor of the disposal vault (Figure 1). A coupled unsaturated flow, chemical reactions, and contaminant transport simulator (STORM) will be used within the near-field (Bacon and McGrail 1997). The plume exiting the region near the vault is expected to be of high ionic strength and pH, and will migrate down into the near-field vadose zone for some distance. However, at some distance from the disposal vaults, geochemical conditions will approach those more typical of the Hanford vadose zone and for which simplifying assumptions (such as linear sorption, negligible precipitation/dissolution, no changes in hydraulic properties, and no density effects) can be used. This region is defined as the far-field environment and can be simulated using standard, nonreactive flow and transport codes. For the ILAW PA, computations in the far-field domain will be done by VAM3DF (Huyakorn and Panday 1995), a variably saturated flow and transport code. The primary reason for switching from the near-field simulator to VAM3DF is to apply a less complicated code for the far-field, and therefore a faster turnaround for the numerical simulations. The radionuclide flux exiting the far-field domain to the unconfined aquifer will be provided by VAM3DF and will be used as a boundary condition for the unconfined aquifer flow and transport simulator. The final step in the methodology is to compute the impacts, if any, from ingestion, inhalation, and external radiation to humans who become exposed to the contaminants by withdrawing water from the aquifer.

1.1 Scope of This Data Package

The scope for the far-field hydrology data package for the new ILAW disposal site and the existing disposal site include the following information:

- Stratigraphic cross-sectional models (Section 2.0). [Note that stratigraphic cross-sectional models are presented for context only; the scope of this data package does *not* include stratigraphic cross-sectional models. Such geologic models shall be provided as part of a separate data package (i.e., Reidel and Horton 1999)]

- Data on laboratory measurements for moisture retention, particle-size distribution, saturated and unsaturated hydraulic conductivity, and bulk density (Section 2.0).
- Effective (upscaled) moisture retention, saturated and unsaturated hydraulic conductivity, bulk density, diffusivity, and macrodispersivity estimates for geologic formations (Section 3.0).

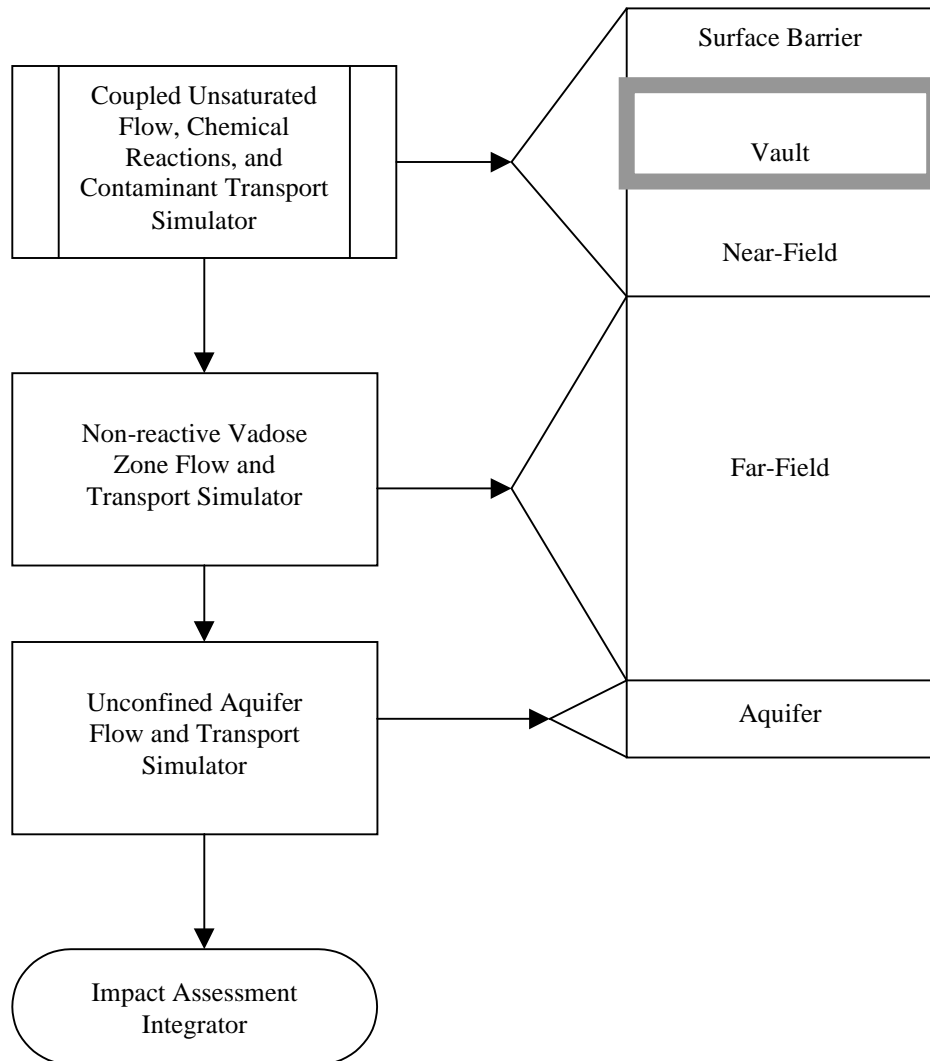


Figure 1. Modeling strategy for assessing ILAW disposal system impacts (after McGrail et al. 1998).

- Sorption-enhanced macrodispersivity estimates for selected radionuclide species (Section 3.0).
- Moisture retention, saturated and unsaturated hydraulic conductivity, bulk density, and macrodispersivity estimates for clastic dike infilling materials (Section 4.0).
- Bounding scenarios on model configurations and uncertainty estimates about the calculated mean concentration and around mean concentration (Section 4.0).

For the ILAW disposal facility with a capillary barrier and a surface barrier on top, the vadose zone water contents beneath the facility are expected to approach the natural moisture regime for arid soils. Field moisture contents are expected to be less than 10% (by volume); matric potentials of the order of -1000 cm and recharge rates of the order of 0.1 cm/yr. Under such arid conditions, the features and processes identified in the scope carry significant importance for the ILAW PA calculations. For example, the layered heterogeneous soils in 200 Areas are expected to show bulk anisotropic behavior, with the hydraulic conductivity parallel to the layers being larger than that normal to the layers. Furthermore, the degree of anisotropy increases rapidly with increasing tension or decreasing moisture content, becoming large in dry soils of the kind expected beneath the disposal facility. Also, the infiltrating water diverted around the vaults by the capillary barrier can potentially move beneath the vaults, creating moist conditions and enhancing contaminant movement to the water table. In addition, recent theoretical work and field experiments have shown that spreading of contaminants undergoing heterogeneous linear equilibrium sorption can be significantly larger than that of the non-sorbing tracer. Dispersivity enhancement can cause early arrival at the water table before they have had an opportunity to decay. Also, clastic dikes are of concern because they can potentially create preferred pathways.

2.0 LABORATORY MEASUREMENTS FOR SOIL PHYSICAL AND HYDRAULIC PROPERTIES

The purpose of this section is to summarize available data on laboratory measurements for moisture retention, particle-size distribution, saturated and unsaturated hydraulic conductivity, and bulk density for sediment samples from both new ILAW and existing disposal sites.

2.1 New ILAW Disposal Site

As part of site characterization activity for the new ILAW disposal site, sediment samples were obtained in fiscal year 1998 via a borehole drilling and sampling program (Reidel and Reynolds 1998). The borehole was drilled in the spring of 1998 (Reidel et al. 1998); Figure 2 shows the geologic cross section. The Hanford formation sandy sequence is about 200 ft thick and is the dominant facies at the site. The lower gravelly sequence is about 70 ft thick. For purposes of this data package, no distinction is made on gravel-dominated sequences of the lower Hanford formation and the upper Ringold Formation. The sediments from both of these formations have similar physical and hydraulic properties, and are characterized essentially as sandy gravel, with a significant gravel fraction (Khaleel and Freeman 1995a,b).

A work plan was prepared that provides details on the measurement and analysis of the hydraulic properties for the ILAW borehole sediment samples (Khaleel 1998)¹. Details on sampling, laboratory procedures, and analysis of samples are provided in Fayer et al. (1998)², and are included as Appendix A. The following summary is based on details provided in Appendix A.

A total of 45 cores were collected in liners, with core diameters ranging from 3.25- to 3.75- in. The total internal volume of the 3.25-in (8.26-cm) diameter cores was 803 cm³; it was 1,069 cm³ for the 3.75-in (9.53-cm) diameter core. It should be noted that, during drilling, sample recovery was less than 100% (Reidel et al. 1998), thereby biasing the recovered samples toward the finer fraction. Also, no vadose zone cores were collected below 242 ft because this zone was open framework gravel (i.e., gravel that supports itself with little to no finer grained material) and could not be sampled with the method used. Figure 2 shows the sampling locations relative to the geologic cross-section derived from the borehole data; twenty samples from these locations were used to obtain physical and hydraulic properties for the sandy sequence. As described later, for the gravel-dominated sequence, data on hydraulic properties from elsewhere on the Hanford Site were used as surrogates.

¹ Khaleel, R. 1998. Work plan for measurement and analysis of hydraulic properties for clastic dikes and ILAW Borehole No. 1 sediment samples. January, 1998. Fluor Daniel Northwest, Inc. Richland, WA.

² Fayer, M.J., A.L. Ward, J.S. Ritter, and R.E. Clayton. 1998. Physical and hydraulic measurements of FY 1998 borehole cores. Letter Report to Fluor Daniel Northwest, Inc. September, 1998. Pacific Northwest National Laboratory. Richland, WA.

The procedures used to analyze the twenty samples are listed in Appendix A. Because several tests were performed on the same core, the following test sequence was established: saturated conductivity, multistep outflow, and steady state unsaturated conductivity. The multistep and steady state methods were used to obtain moisture retention and unsaturated conductivity data. Both methods were performed on the same core using the same sensor locations (see Appendix A for details). In addition to cumulative outflow, the multistep method, which is an improvement over the one-step method of Kool et al. (1985a, b), provides water content-matric potential (θ - ψ) pairs. These data were used in conjunction with the MULSTP program (Eching and Hopmans 1993), a numerical inversion procedure, to determine the optimal set of van Genuchten model (Appendix A) parameters. The steady-state method, described by Klute and Dirksen (1986), provides water content-matric potential-unsaturated conductivity (θ - ψ - K) triplets; the method was primarily used as a check on the multistep method.

Table 1 shows the van Genuchten model (van Genuchten 1980) parameters determined using the MULSTP program and data from the multistep test. The pore-size distribution parameter n (Mualem 1976) was kept fixed at 0.5. Also listed in Table 1 are saturated conductivity and bulk density measurements for the 20 samples primarily from the sandy sequence. The particle-size distribution data are shown in Figure 3. The fitted moisture retention curves and unsaturated conductivity curves for the 20 samples from the sandy sequence are shown in Figure 4. Most of the borehole samples were fitted for n and α ; eight of the samples were also fitted for α_s .

2.1.1 100 Area Samples

As discussed earlier, no site-specific data on soil moisture characteristics are available at the disposal sites for sediments in the gravel-dominated sequence. However, as part of the Environmental Restoration Project, moisture retention and unsaturated conductivity data for sandy gravel sediments are available elsewhere (100 Area along the Columbia River) on the Hanford Site. Fifteen samples having a large gravel fraction were chosen. These samples ranged in gravel content from 43 to 75 percent and were used as surrogate to represent the hydraulic properties for the gravel-dominated sequence.

Standard laboratory and Westinghouse Hanford Company quality assurance procedures were used to analyze these gravelly samples. The moisture retention data for the fine fraction (< 2 mm) and for the drainage cycle of up to -1,000 cm of pressure head were measured using "Tempe" pressure cells; the rest of the drainage data up to -15,000 cm was measured using the pressure plate extraction method (Klute 1986). Saturated hydraulic conductivities for the bulk samples (including gravels) were measured in the laboratory using constant-head permeameter. A variation of the unit gradient method (Klute and Dirksen 1986; Khaleel et al. 1995) was used to measure unsaturated hydraulic conductivities for the bulk samples. The laboratory measured data on < 2 mm size fraction were corrected for the gravel fraction (Gardner 1986; Khaleel and Relyea 1997).

No correction was needed for the saturated and unsaturated conductivities, since these were measured on the bulk sample.

The van Genuchten parameters were obtained via RETC (van Genuchten et al. 1991) and a simultaneous fit of both laboratory-measured moisture retention and unsaturated conductivity data; all five unknown parameters θ_r , θ_s , α , n , and K_s , with $m=1-1/n$ (van Genuchten 1980), were fitted to the data. The pore size distribution factor, λ (Mualem 1976) was kept fixed at 0.5 during the simultaneous fitting. The laboratory data, following gravel-correction of the moisture retention data, are included in Appendix B for the 15 samples. Appendix B serves as the input data file for RETC. The fitted moisture retention curves and unsaturated conductivity curves for the 15 samples for the gravel sequence are shown in Figure 5. Note that, unlike the borehole samples, the 100 Area samples were fitted for θ_r , θ_s , α , n , and K_s .

Table 1. Van Genuchten parameters (based on the multistep method), saturated hydraulic conductivity, and bulk density data for 20 ILAW borehole samples from the sandy sequence (after Fayer et al. 1998).

Sample	θ_s (cm ³ /cm ³)	θ_r (cm ³ /cm ³)	α (1/cm)	n (-)	Saturated Hydraulic Conductivity (cm/s)	Bulk Density (g/cm ³)
7A	0.377	0.0404	0.0290	1.825	1.04E-03	1.70
10A	0.413	0.0279	0.1161	1.784	2.95E-03	1.62
12A	0.363	0.0309	0.0650	1.755	2.15E-03	1.74
14A	0.416	0.0324	0.0445	1.728	1.99E-03	1.58
15A	0.380	0.0254	0.0487	1.844	2.09E-03	1.69
16A	0.420	0.0228	0.0682	1.710	9.57E-03	1.58
17A	0.423	0.0382	0.0689	1.899	1.99E-03	1.57
19A	0.444	0.0279	0.2010	1.542	4.31E-03	1.52
20A	0.419	0.0321	0.0305	2.081	2.54E-03	1.58
21A	0.403	0.0276	0.0545	1.926	2.94E-03	1.62
22A	0.352	0.0252	0.1078	1.585	5.06E-03	1.78
23A	0.371	0.0411	0.0079	1.553	2.65E-04	1.72
24A	0.321	0.0413	0.0130	1.684	5.69E-04	1.85
25A	0.345	0.0267	0.0842	2.158	5.40E-03	1.80
27A	0.377	0.0354	0.0830	1.532	8.14E-03	1.71
29A	0.359	0.0317	0.0784	1.732	3.75E-03	1.76
31A	0.418	0.0444	0.0058	2.012	8.21E-04	1.60
32A	0.359	0.0401	0.0931	1.703	6.71E-03	1.78
34A	0.316	0.0324	0.0819	2.398	1.32E-02	1.92
35A	0.299	0.0428	0.0897	2.160	1.06E-02	1.98

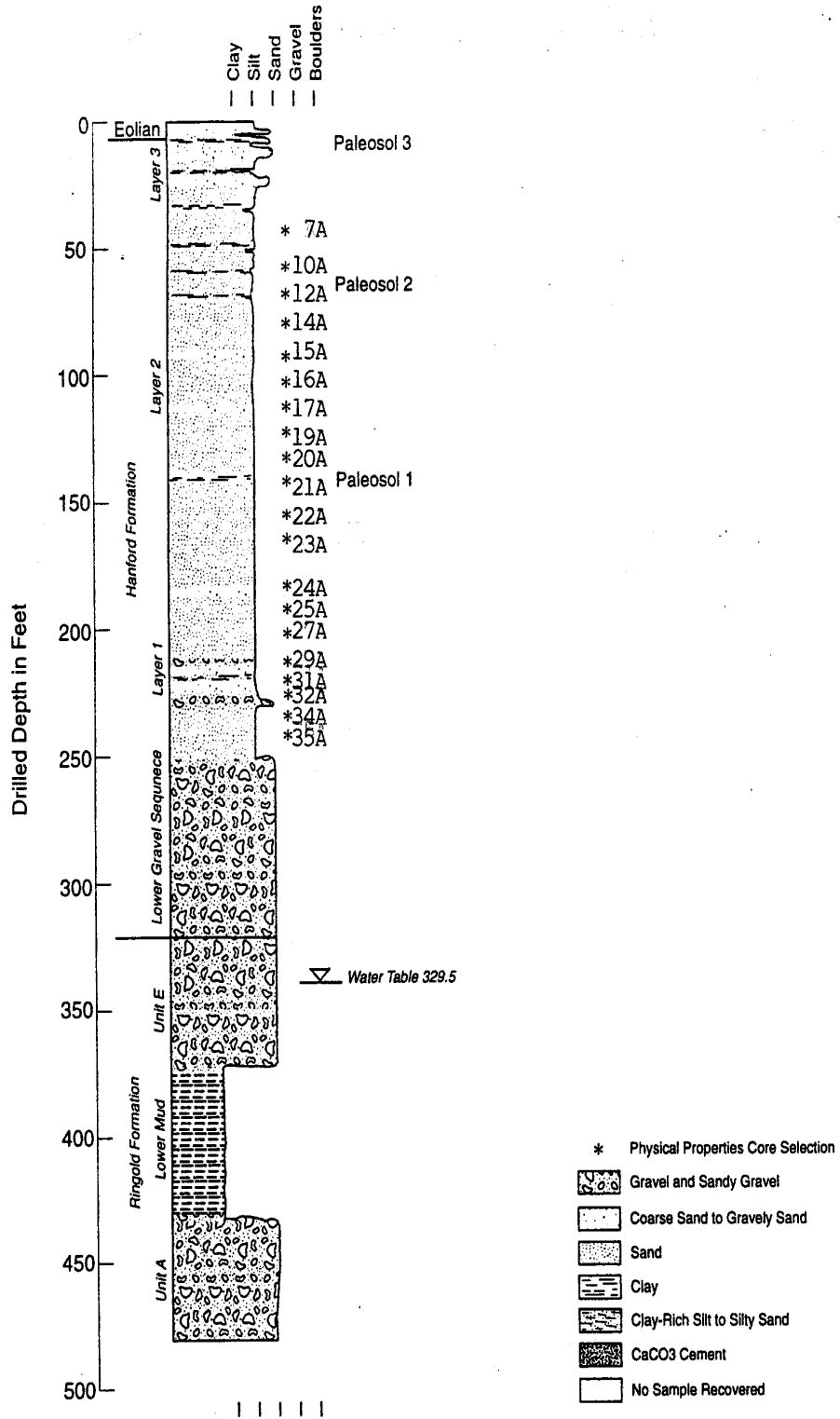


Figure 2. Geologic cross section of the new ILAW disposal site (after Reidel et al. 1998).

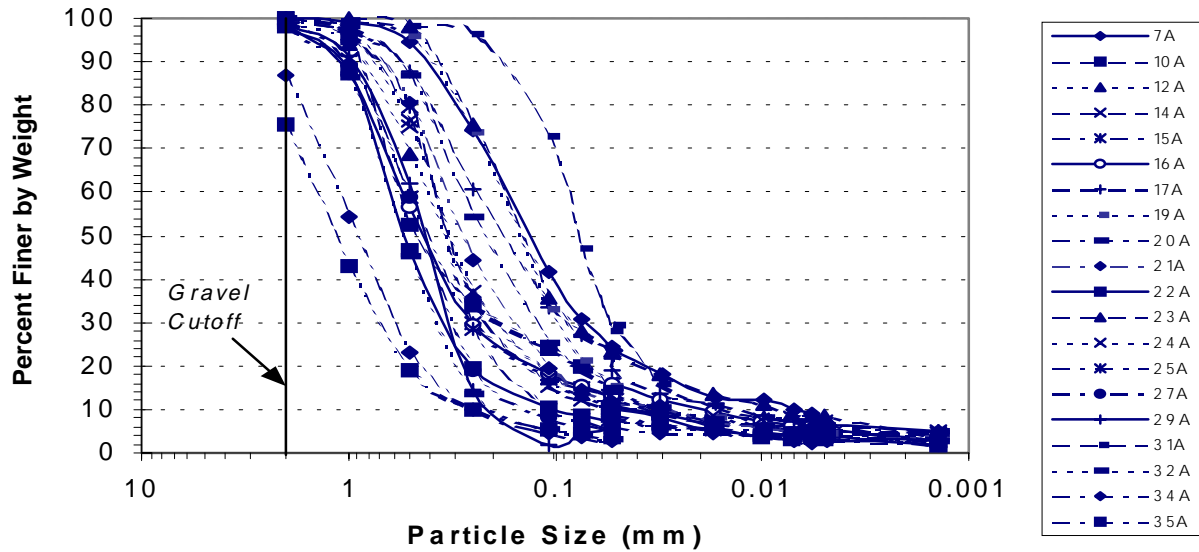


Figure 3. Particle-size distribution for 20 samples from the sand-dominated sequence at the new ILAW disposal site.

Table 2. Van Genuchten parameters, fitted saturated hydraulic conductivity, and measured bulk density data for 15 sandy gravel samples.

Sample	Operable Unit	Well Number	Depth (m)	Percent Gravel	θ_s (cm ³ /cm ³)	θ_r (cm ³ /cm ³)	α (1/cm)	n (-)	Fitted K_s (cm/s)	Bulk Density (g/cm ³)
2-1307	100-HR-3	199-D5-14	18.90	43	0.236	0.0089	0.0130	1.447	1.29E-04	2.15
2-1308	100-HR-3	199-D5-14	30.64	58	0.120	0.0208	0.0126	1.628	6.97E-05	2.13
2-1318	100-HR-3	199-D8-54A	15.54	60	0.124	0.0108	0.0081	1.496	1.67E-04	2.16
2-2663	100-BC-5	199-B2-12	8.20	61	0.135	0.0179	0.0067	1.527	6.73E-05	2.38
2-2664	100-BC-5	199-B2-12	24.84	73	0.125	0.0136	0.0152	1.516	1.12E-04	2.25
2-2666	100-BC-5	199-B4-9	21.49	71	0.138	0.00	0.0087	1.284	1.02E-04	2.10
2-2667	100-BC-5	199-B4-9	23.93	75	0.094	0.00	0.0104	1.296	1.40E-04	2.16
3-0570	100-KR-1	116-KE-4A	3.50	60	0.141	0.00	0.0869	1.195	2.06E-02	2.12
3-0577	100-FR-3	199-F5-43B	7.16	66	0.107	0.00	0.0166	1.359	2.49E-04	2.32
3-0686	100-FR-1	116-F-14	6.49	55	0.184	0.00	0.0123	1.600	5.93E-04	2.17
3-1702	100-DR-2	199-D5-30	9.78	68	0.103	0.00	0.0491	1.260	1.30E-03	2.33
4-1086	100-K	199-K-110A	12.77	65	0.137	0.00	0.1513	1.189	5.83E-02	2.26
4-1090	100-K	199-K-111A	8.20	50	0.152	0.0159	0.0159	1.619	4.05E-04	2.21
4-1118	100-K	199-K-109A	10.30	66	0.163	0.00	0.2481	1.183	3.89E-02	2.12
4-1120	100-K	199-K-109A	18.90	63	0.131	0.0070	0.0138	1.501	2.85E-04	2.06

2.2 Existing Disposal Site

The geologic cross-section in the vicinity of the existing disposal site is shown in Figure 6 (Kincaid et al. 1995). The cross-section appears to be very similar to that of the new ILAW disposal site. Again, for purposes of this data package, no distinction is made on gravel-dominated sequences of the lower Hanford formation and the Ringold Formation. Physical and hydraulic properties' information on sediments from borehole 299-E25-234 was obtained. Such information included particle-size distribution, bulk density, moisture retention, and saturated hydraulic conductivity. Unlike the new ILAW site, notably absent were any measurements of unsaturated hydraulic conductivity. It is, however, well recognized that estimated unsaturated conductivities, based on saturated conductivity and the van Genuchten retention model, can differ by up to several orders of magnitude with measured conductivities at the dry end (e.g., Khaleel et al. 1995). Therefore, it was decided to use, as much as possible, the new ILAW site sediment properties for the existing disposal site, since the geology for the two sites is not significantly different and measurements of both moisture retention and unsaturated conductivity are available for sediments at the new ILAW site. In fact, the average particle-size distribution for the sandy sequence sediments at the two sites is very similar: <1% gravel, 91% sand, 9% silt and clay for the existing disposal site and <2% gravel, 88% sand, 10% silt and clay for the new ILAW site. Similar to the new ILAW site, the gravel-dominated sequence at the existing disposal site is comprised primarily of sandy gravel. In summary, as indicated in Table 3, the soil physical and hydraulic properties at the new ILAW and existing disposal sites are similar.

Table 3. Comparison of mean parameter estimates for the sandy sequence at the new ILAW and existing disposal sites.

Parameter	New ILAW Disposal Site	Existing Disposal Site
θ_s	0.379	0.420
θ_r	0.033	0.023
K_s (geometric mean), cm/sec	0.0029	0.0016
Bulk Density, g/cm^3	1.71	1.58

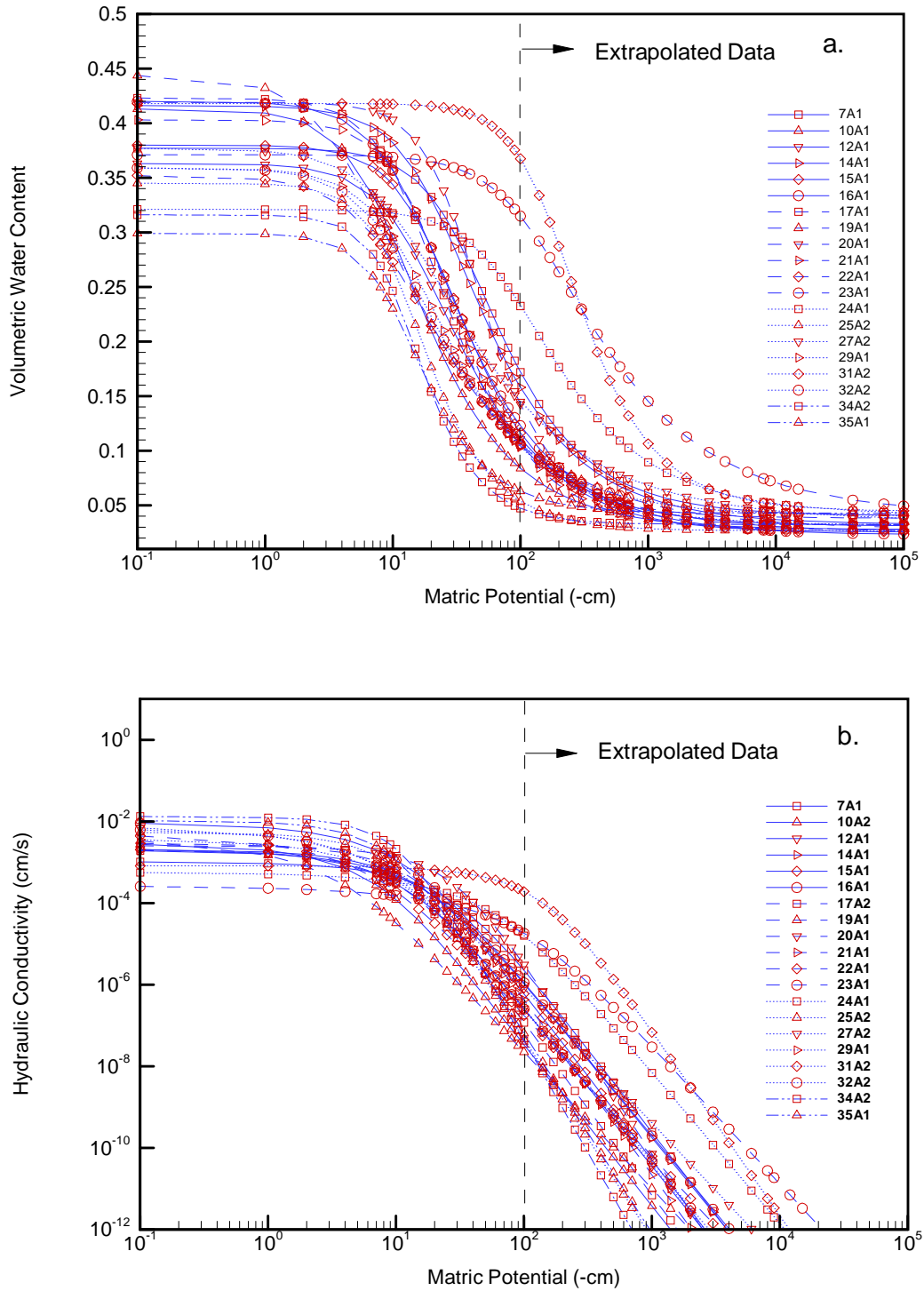


Figure 4. Fitted moisture retention and unsaturated conductivity curves for 20 samples for the sand-dominated sequence (the symbols represent various samples, not experimental data).

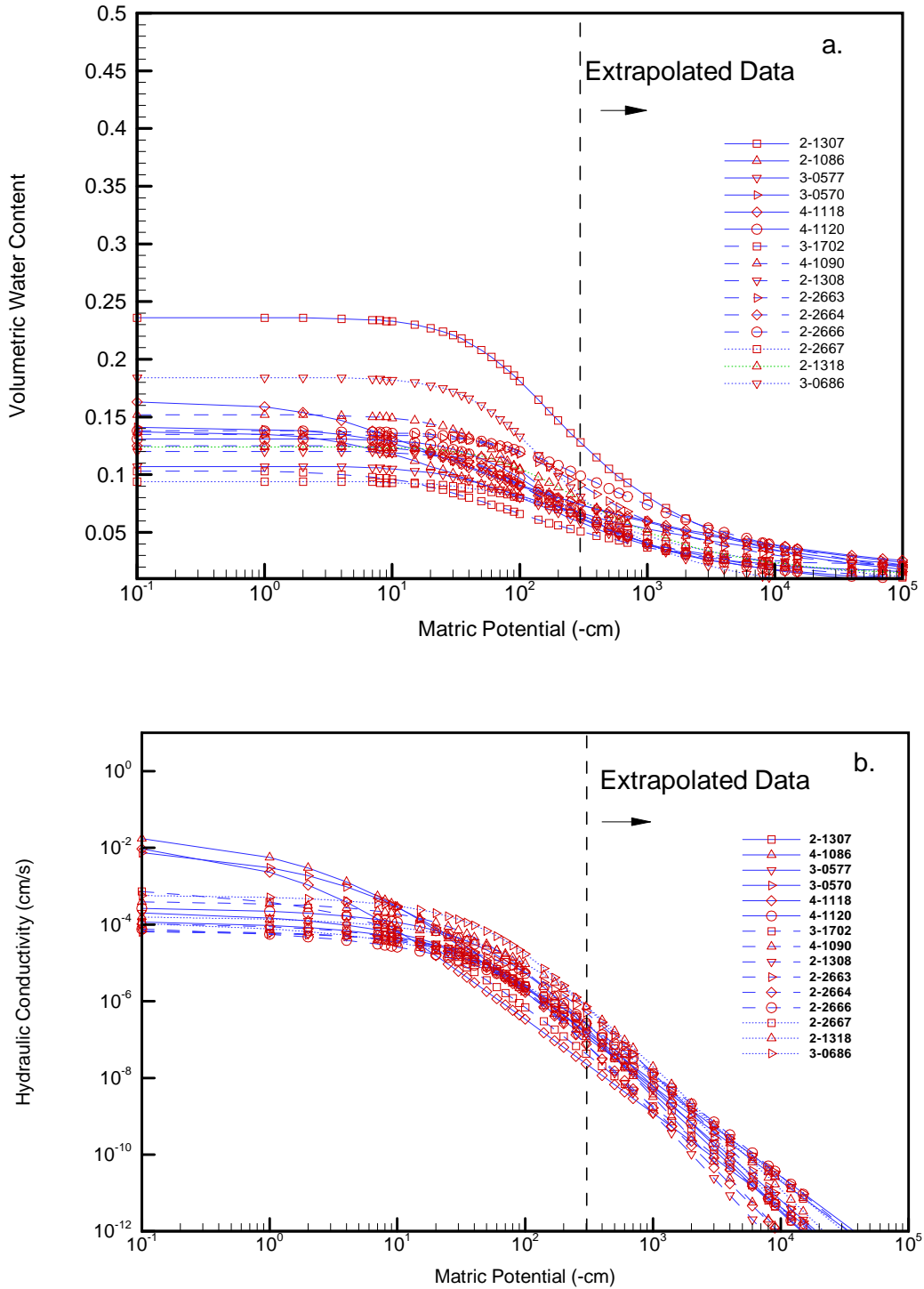


Figure 5. Fitted moisture retention and unsaturated conductivity curves for 15 samples for the gravel-dominated sequence (the symbols represent various samples, not experimental data).

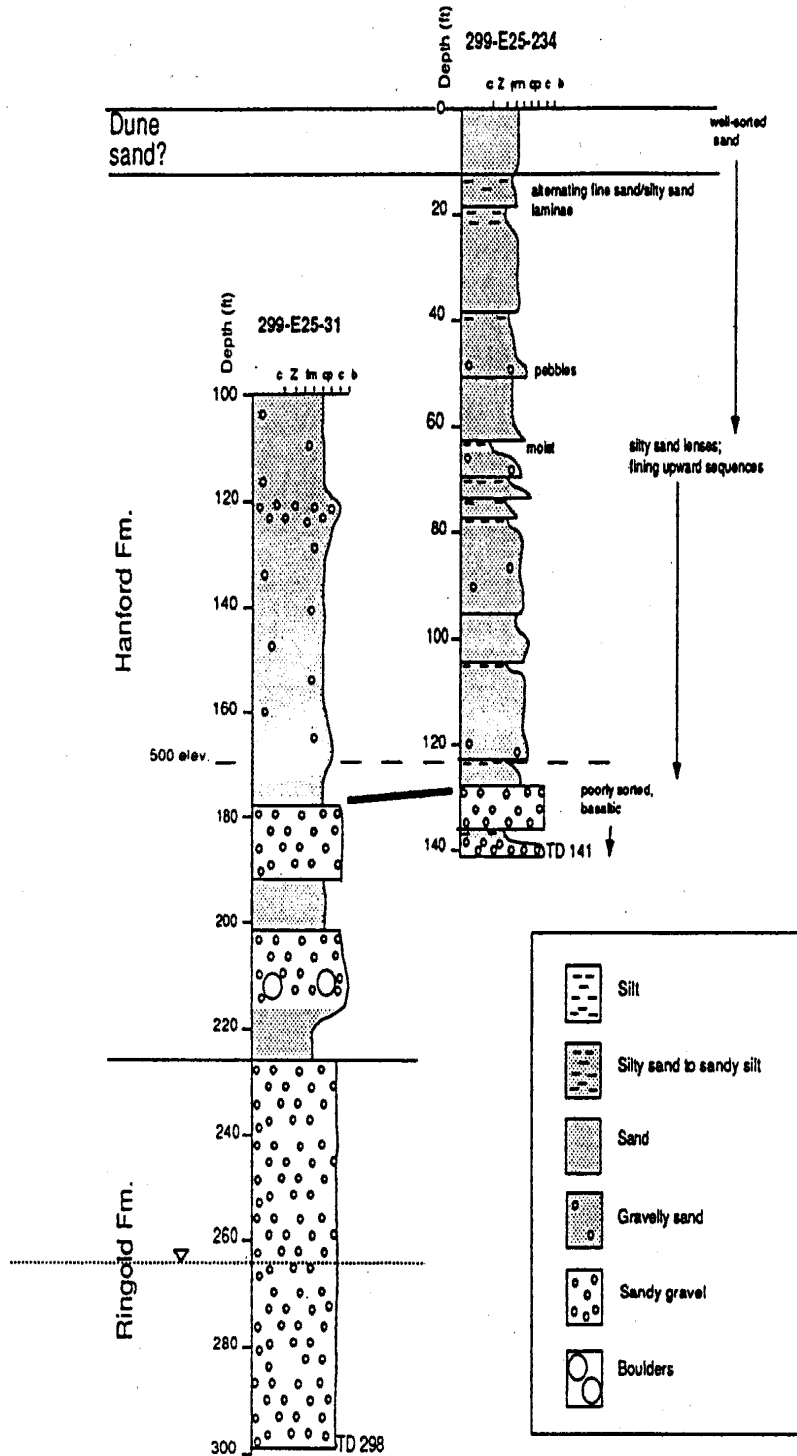


Figure 6. Geologic cross section of the existing disposal site (after Kincaid et al. 1995).

3.0 EFFECTIVE (UPSCALED) FLOW AND TRANSPORT PROPERTIES

Data on hydraulic properties, described in the preceding section, were obtained via laboratory tests on core samples (scales of the order of a few cm). However, numerical models of fluid flow and contaminant transport in the unsaturated zone require specifying hydraulic properties for each discretized grid block (scales of the order of meters). Therefore, the scale of the grid blocks is usually much larger than the scale at which the unsaturated properties were measured. The process of defining large-scale properties for the numerical grid blocks based on small, measurement-scale point measurements is called upscaling.

This section provides effective (upscaled) values of flow and transport parameters for the far-field vadose zone. Specific flow parameters include moisture retention, saturated and unsaturated hydraulic conductivity. Transport parameters include bulk density, diffusivity, and macrodispersivity. Sorption coefficients are included as part of another data package.

3.1 Effective (Upscaled) Flow Parameters

Any attempt at upscaling is confronted with the issue of spatial variability of hydraulic properties due to small-scale soil heterogeneities. The presence of spatial variability in hydraulic properties of Hanford soils has been well documented (e.g., Khaleel and Freeman 1995a). A fundamental issue is then how best to incorporate the effects of natural heterogeneity in modeling. A traditional approach is to use deterministic models and attempt to incorporate the overall heterogeneity of the system such as layering while neglecting the small-scale heterogeneity. The considerable spatial variability of Hanford soils makes complete characterization of the hydraulic properties at the field scale an almost impossible task, as an enormous amount of data is required for proper representation of the actual media heterogeneities.

An alternative approach is to define an equivalent homogeneous medium with average, effective (upscaled) hydraulic properties that are related to the local small-scale heterogeneities and thereby predict the mean flow and transport behavior of the field-scale, larger media. However, to represent a heterogeneous medium by its homogeneous equivalent, we need to estimate the effective hydraulic properties that represent this equivalent homogeneous medium. A straightforward approach would be to use statistical averages (arithmetic or geometric) of the local soil hydraulic properties, but such simple estimates may not always be able to properly describe the complicated nonlinear behavior in heterogeneous soils.

3.1.1 Stochastic Upscaling

For saturated media, an averaging of the heterogeneities in geologic media at a smaller scale leads to an effective hydraulic conductivity value, at the larger (macroscopic) scale, with the lateral hydraulic conductivity being much larger than the vertical conductivity (Freeze and Cherry 1979). For unsaturated media, theoretical (e.g., Mualem 1984, Yeh et al. 1985a, b; c, Bear et al. 1987; Mantoglou and Gelhar 1987; Green and Freyberg 1995) and experimental analyses (e.g., Stephens and Heerman 1988; Yeh and Harvey 1990; McCord et al. 1991) of field-scale unsaturated flow indicates that in stratified sediments, the effective hydraulic conductivity tensor is anisotropic with a tension-dependent (or moisture-dependent) degree of anisotropy. The anisotropy ratio of horizontal hydraulic conductivity to vertical hydraulic conductivity increases with decreasing moisture content. Variable, moisture-dependent anisotropy in unsaturated soils is therefore an effective, large-scale (macroscopic) flow property which results from media heterogeneities at a smaller scale, and provide a framework for upscaling laboratory-scale measurements to the effective (upscaled) properties for the large-scale vadose zone.

3.1.2 Field Observations

Field observations in the vicinity of the new ILAW and existing disposal sites do indeed provide evidence of saturation-dependent anisotropy and lateral migration. A test facility comprising an injection well at the center and a radial array of 32 monitoring wells was constructed in 1980 south of PUREX in 200 East Area. The facility was used in late 1980 and early 1981 to conduct an infiltration and multiple tracer (i.e., chloride, nitrate, barium, rubidium, Sr-85 and Cs-134) test, in which 45,000 L of liquid (in 11 increments) were injected at a depth of 4.7 m over a period of 133 days (Sisson and Lu 1984). Three-dimensional water content profiles in layered, coarse sediments were monitored to a depth of 18 m by down-hole neutron probe measurements. The initial water contents were measured at 30-cm increments over the 30- to 1800-cm depths in all 32 observation wells. In situ gamma energy analysis data were collected to determine the distribution of radioactive tracers. The unique three-dimensional nature of the experiment and the measured water content profiles provide evidence of tension-dependent anisotropy. The field data clearly show lateral spreading that occurred during injection. The horizontal wetting patterns dominated the experiment. In fact, numerical modeling results (Sisson and Lu 1984), based on the assumption of a uniform and isotropic model, showed a much deeper penetration of the moisture profile than occurring in the field (Sisson and Lu 1984). The degree of spreading was remarkable considering the apparent uniform lithology at the site.

3.1.3 Composite Macroscopic Relationships

Figures 4 and 5 show that moisture retention data show spatial variability, although the degree of variation at a given tension is more modest than that of hydraulic conductivity. Based on data in Tables 1 and 2, composite parameters for the moisture retention

relations were determined. For both sandy and gravelly soils, the composite van Genuchten parameters were obtained via RETC (van Genuchten et al. 1991) and a simultaneous fit of both moisture retention and unsaturated conductivity predictions; all four unknown parameters α_r , α_s , α , and n with $m=1-1/n$ (van Genuchten 1980), were fitted to the data. The pore size distribution factor α was kept constant at 0.5 during the simultaneous fitting. The saturated conductivity, K_s , was also kept constant as geometric mean of the sample estimates.

The fitted composite moisture retention and unsaturated conductivity curves are shown as Figures 7 and 8, respectively, for the sandy and gravelly sequences. Table 3 shows the fitted parameters. Equivalent horizontal and vertical hydraulic conductivities are derived using macroscopic anisotropy relations.

Table 4. Composite van Genuchten-Mualem parameters for the sand- and gravel-dominated sequences.

Formation	Number of samples	α_s	α_r	α (1/cm)	n	α	K_s (cm/s)
Sandy	20	0.375	0.041	0.057	1.768	0.5	2.88E-03
Gravelly	15	0.138	0.010	0.021	1.374	0.5	5.60E-04

3.1.3.1 Stochastic Model for Macroscopic Anisotropy

As discussed earlier, variable, tension-dependent anisotropy provides a framework for upscaling small-scale measurements to the effective (upscaled) properties for the large-scale vadose zone. A stochastic model is used to evaluate tension-dependent anisotropy for sediments at the new ILAW site.

Yeh et al. (1985b) analyzed steady unsaturated flow through heterogeneous porous media using a stochastic model; parameters such as hydraulic conductivity are treated as random variables rather than as deterministic quantities. The Gardner (1958) relationship was used by Yeh et al. to describe unsaturated hydraulic conductivity (K) as a function of saturated hydraulic conductivity (K_s) and tension (ψ), i.e.,

$$K(\psi) = K_s \exp(-\beta\psi) \quad (1)$$

where β is a fitting parameter. Equation (1) can be written as

$$\ln K(\psi) = \ln K_s - \beta\psi \quad (2)$$

Equation (2) is referred to as the log-linear model, since $\ln K$ is linearly related to ψ through the constant slope p . However, such a constant slope is often inadequate in describing $\ln K(\psi)$ over ranges of tension of practical interest for field applications. As an alternative, the slope p can be approximated locally by straight lines over a fixed range of tension. The " $\ln K_s$ " term in equation (2) can then be derived by extrapolating the local slopes back to zero tension.

Using a linear correlation model between the log-conductivity zero-tension intercept and ψ , Polmann (1990) presents a generalized model that accounts for the cross-correlation of the local soil property (i.e., $\ln K_s$ and ψ) residual fluctuations. Compared to uncorrelated $\ln K_s$ and ψ model, partial correlation of the properties is shown to have a significant impact on the magnitude of the effective parameters derived from the stochastic theory. The Polmann (1990) equations for deriving the effective parameters are as follows.

$$\begin{aligned} \langle \ln K \rangle &= \langle \ln K_s \rangle - A \langle \psi \rangle - \sigma_{\ln K_s}^2 \lambda [p - p^2 \langle \psi \rangle - \zeta^2 \langle \psi \rangle] / (1 + A\lambda) \\ \sigma_{\ln K}^2 &= \sigma_{\ln K_s}^2 [(1 - p \langle \psi \rangle)^2 + \zeta^2 \langle \psi \rangle^2] / (1 + A\lambda) \\ K_h^{eq} &= \exp[\langle \ln K \rangle + (\sigma_{\ln K}^2 / 2)] \\ K_v^{eq} &= \exp[\langle \ln K \rangle - (\sigma_{\ln K}^2 / 2)] \end{aligned} \quad (3)$$

where $\sigma_{\ln K}^2$ = variance of log unsaturated conductivity (which depends on mean tension),

$\langle \psi \rangle$ = mean tension,

$\sigma_{\ln K_s}^2$ = variance of $\ln K_s$

$\langle \ln K_s \rangle$ = mean of $\ln K_s$,

p = slope of the ψ versus $\ln K_s$ regression line,

$\zeta = \sigma_{\psi} / \sigma_{\ln K_s}$,

σ_{ψ} = standard deviation of the residuals in the ψ versus $\ln K_s$ regression,

A = mean slope, ψ , for $\ln K_s$ vs. ψ ,

λ = vertical correlation lengths for $\ln K_s$ (assumed to be same as that of ψ),

K_h^{eq} = equivalent unsaturated horizontal conductivity, and

K_v^{eq} = equivalent unsaturated vertical conductivity.

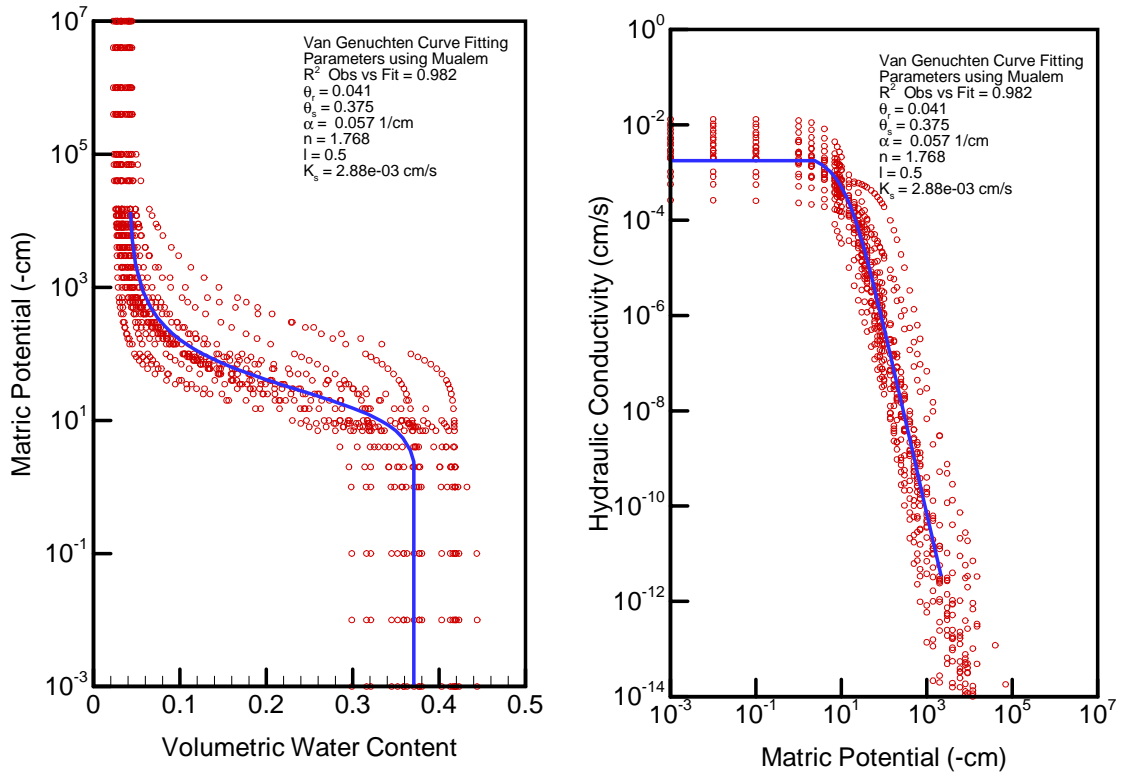


Figure 7. Composite moisture retention and unsaturated conductivity curves for the sand-dominated sequence.

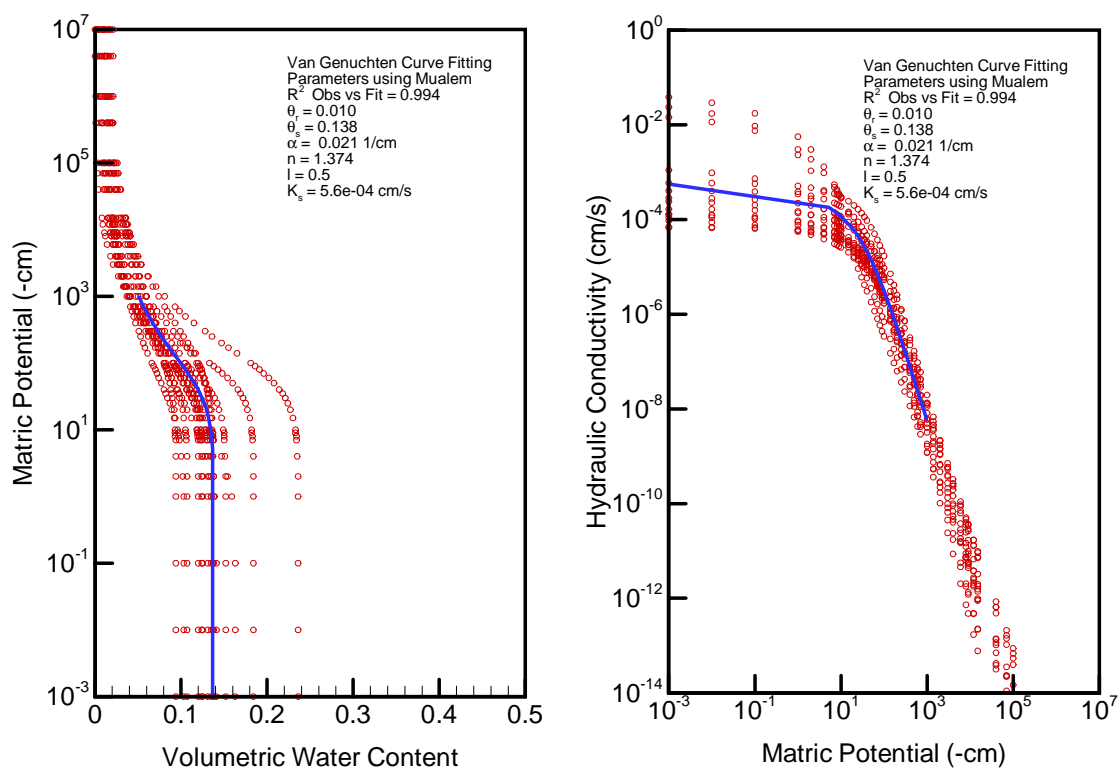


Figure 8. Composite moisture retention and unsaturated conductivity curves for the gravel-dominated sequence.

3.1.3.2 Macroscopic Anisotropy Relations

Results of application of equation (3) for variable anisotropy are presented below. The same 20 samples (Table 1) of the sandy sequence were used to obtain parameters $\langle \ln K_s \rangle$, $\sigma_{\ln K_s}^2$, p , \bullet , and A . The slope and pseudo $\ln K_s$ estimates, discussed in the preceding section, were evaluated for the moisture regime of interest (i.e., tension range of 500 cm to 700 cm for the sandy sequence and 700 cm to 1000 cm for the gravelly sequence). It should be noted, however, that no experimental data are available for unsaturated conductivities in the tension range of interest; \bullet and $\ln K_s$ estimates were based on the fitted van Genuchten-Mualem curves (Figures 7 and 8). The tension ranges are consistent with a base case recharge estimate of about 0.1 cm/yr (Figures 7 and 8).

An estimate of the correlation length, \bullet , is needed for anisotropy calculations. Most of the measurements in the vicinity of the ILAW site have been obtained at sampling intervals that are too coarse to yield a reasonable estimate for the correlation length. However, one data set is available that provides saturated conductivity estimates at about 30 cm intervals for a depth of 18 m within the Hanford formation; the site is located about 1/2 mile east of the ILAW site. Figure 9 shows the experimental variogram and the

fitted spherical variogram model for saturated conductivities. The fitted spherical variogram suggests a correlation length, \bullet , of about 50 cm; i.e., the distance at which the variogram drops to $[1-(1/e)]$ times the sill (Figure 9). The correlation length, \bullet , for both $\ln K_s$ and \bullet were assumed to be equal.

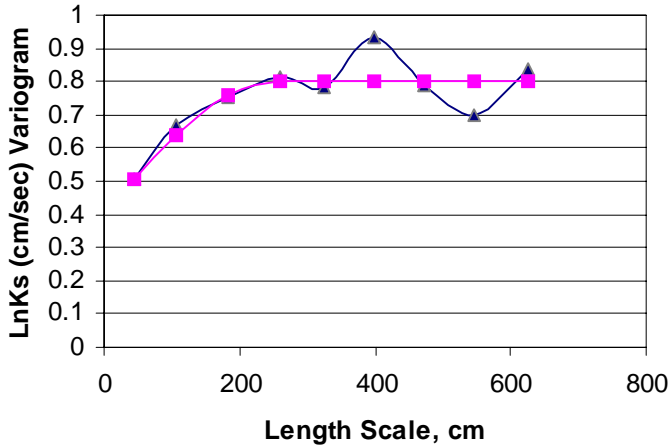


Figure 9. Experimental (triangles) and fitted theoretical (squares) variogram for $\ln K_s$.

The Polmann parameters for both sandy and gravel-dominated sequences are shown in Table 5. Note that, compared to the sandy soils, mean slope, A , $\langle \ln K_s \rangle$, $\sigma_{\ln K_s}^2$, and \bullet values for the gravelly soils are significantly lower; \bullet for the gravelly samples was also almost two orders of magnitude lower. Because of these different characteristics, the macroscopic anisotropy relations for the sandy and gravelly sediments are quite different. Figures 10 and 11 illustrate the macroscopic anisotropy relations for the two sediments. The anisotropy for the gravelly soils is much less compared to that for sandy soils. In fact, for the tension range of interest for ILAW PA modeling, anisotropy ratio is about two. Note that, for gravelly soils, no data were available for a variogram analysis. However, a smaller \bullet value (30 cm) is used (Table 5) because of a much higher variance of $\ln K_s$ for the gravelly soils than for the sandy soils.

Table 5. Macroscopic anisotropy parameters for the sand- and gravel-dominated sequences.

Formation	Number of samples	$\langle \ln K_s \rangle$	$\sigma_{\ln K_s}^2$	p	\bullet	\bullet (cm)	A
Sandy	20	-17.3	2.89	-1.4E-4	3.18E-4	50	0.00680
Gravelly	15	-15.6	1.03	1.9E-4	4.24E-4	30	0.00354

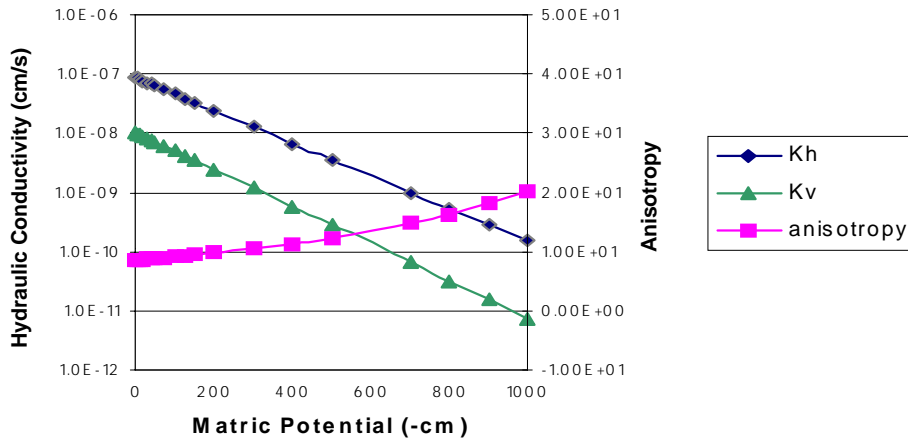


Figure 10. Calculated macroscopic anisotropy (equation 3) as a function of mean pressure head for the sand-dominated sequence.

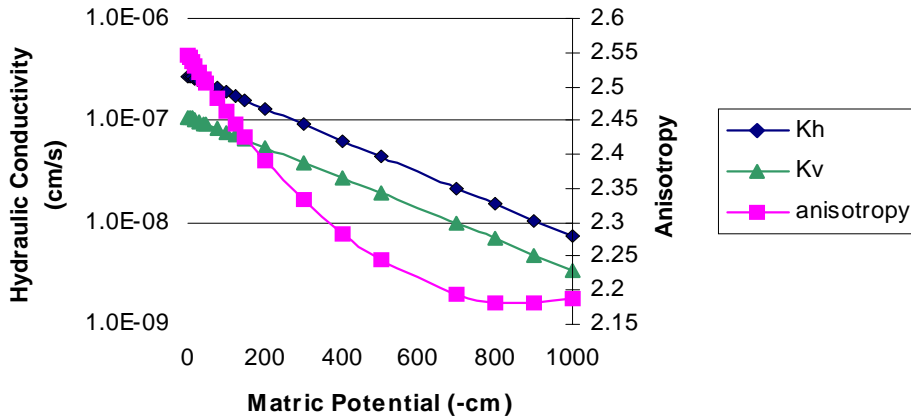


Figure 11. Calculated macroscopic anisotropy (equation 3) as a function of mean pressure head for the gravel-dominated sequence.

3.2 Effective Transport Parameters

Base case effective transport parameter (bulk density, diffusivity, and dispersivity) estimates are presented in this section. Because of natural variability, the transport parameters are all spatially variable. The purpose is again, similar to the flow parameters, to evaluate the effect of such variability on the large-scale transport process.

3.2.1 Bulk Density

Both bulk density (ρ_b) and K_d estimates are needed to calculate retardation factors for different species. The effective, large-scale estimate for the product [$\rho_b K_d$] is the average of the product of small-scale laboratory measurements for bulk density and K_d (Gelhar 1993). The laboratory measurements for ρ_b are shown in Tables 1 and 2, respectively, for the sandy and the gravel-dominated sequences, whereas the K_d measurements are available in Kaplan et al. (1998). Table 6 provides the effective, large-scale estimates.

Table 6. Effective parameter estimates, $E[\rho_b K_d]$, for the product of bulk density (g/cm^3) and K_d (cm^3/g) at the new ILAW and existing disposal sites.

Species	$E[\rho_b K_d]$	
	Sandy	Gravelly
Cs	3473	1700
Sr	25.20	12.20
U	1.05	0.51
Se	11.32	5.56

3.2.2 Diffusivity

It is assumed that the effective, large-scale diffusion coefficients for both sandy and gravel-dominated sequences at both sites are a function of volumetric moisture content, θ . VAM3DF uses the Millington-Quirk (1961) empirical relation:

$$D_e(\theta) = D_0 \frac{\theta^{10/3}}{\theta_s^2} \quad (4)$$

where $D_e(\theta)$ is the effective diffusion coefficient of an ionic species, and D_0 is the effective diffusion coefficient for the same species in free water. The molecular diffusion coefficient for all species in pore water is assumed to be $2.5 \times 10^{-5} \text{ cm}^2/\text{sec}$ (Kincaid et al. 1995).

3.2.3 Dispersivity

An extended review is provided on the rationale of choice for vadose zone dispersivity estimates. Readers who are familiar with the state-of-the-art can proceed directly to Section 3.2.3.4.

A variety of factors such as the size of the flow domain, the flow regime (saturated versus unsaturated flow), field heterogeneities, and the contaminant species (retarded versus nonretarded) need to be recognized in estimating dispersivities. The objective of this section is to provide appropriate guidance on the choice of vadose zone dispersivity estimates for use in ILAW PA.

It should be noted that laboratory data would be of little use in estimating field-scale dispersivities. While well-designed, large-scale tracer experiments would provide useful information, limited field data are available at this time. Therefore, the dispersivity estimates needed for modeling are essentially based on literature values and the available stochastic equations.

Literature data suggest that much more information is available on dispersion in saturated media than in unsaturated media. Therefore, first the available data on dispersivities in saturated media are summarized (Gelhar et al. 1992). Second, available data on vadose zone dispersivities are presented, including results of small-scale tracer experiments in the vicinity of the new ILAW site in 200 East Area. Third, the stochastic framework used in obtaining dispersivity estimates is reviewed, and estimates are provided for use in ILAW PA.

3.2.3.1 Saturated Media Dispersivities For Field Sites

A critical review of dispersivity observations from 59 different field sites was performed by Gelhar et al. (1992). Extensive tabulations of information were included by Gelhar et al. on aquifer type, hydraulic properties, flow configuration, type of monitoring network, tracer, method of data interpretation, overall scale of observation and longitudinal, horizontal transverse and vertical transverse dispersivities from original sources. The information was then used to classify the dispersivity data into three reliability classes: low, intermediate, and high. Overall, the data indicate a trend of systematic increase of the longitudinal dispersivity with observation scale but the trend is much less apparent when the reliability of data (Figure 12) is considered. The longitudinal dispersivity ranged from 10^{-1} to 10^5 m, but the largest scale for high reliability data was only 250 m. When the data are classified according to porous versus fractured media, no significant differences were apparent between these aquifer types. At a given scale, the longitudinal dispersivity values were found to range over 2 to 3 orders of magnitude and the higher reliability data approached the lower portion of this range. The high reliability dispersivity data ranged from a low of about 0.6 m at a scale of 15 m to about 1 m at a scale of 250 m; some data are on the order of 2 to 3.5 m at a scale of 30 m (Figure 12). It is not appropriate to represent the longitudinal dispersivity data by a single universal line.

The variations in dispersivity reflect the influence of differing degrees of aquifer heterogeneity at different sites. The data on transverse dispersivities are more limited but clearly indicate that vertical transverse dispersivities are typically an order of magnitude smaller than horizontal transverse dispersivities (Gelhar et al. 1992). Reanalysis of data from several of the field sites showed that improved interpretations most often lead to smaller dispersivities (Gelhar et al. 1992). Overall, Gelhar et al. concluded that longitudinal dispersivities in the lower part of the indicated range are more likely to be realistic for field situations. This suggests that, for conservative species, a longitudinal dispersivity of the order of a meter is a reasonable estimate for saturated media domains that are a couple of hundred meters in scale. Note that the estimates are for saturated media and conservative species. As discussed later, dispersivity estimates are enhanced due to heterogeneous sorption in both saturated and unsaturated media.

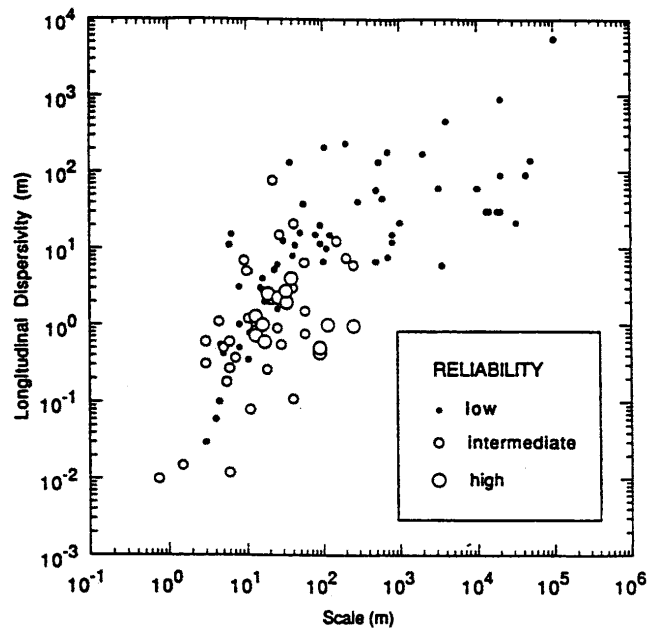


Figure 12. Longitudinal macrodispersivity in saturated media as a function of overall problem scale with data classified by reliability (after Gelhar et al. 1992).

3.2.3.2 Vadose Zone Dispersivities For Dry Desert Environment

As discussed earlier, for an engineered waste disposal facility with a capillary barrier and a surface barrier on top, the vadose zone water contents beneath the disposal facility are expected to approach the natural moisture regime for arid soils. Although exceptional precipitation events may cause transient high water contents near the soil surface, the source of the infiltration is not likely to be sustained at great depths within the vadose zone.

This inference is supported by the results of artificial tracer experiments on much shorter time scales. For example, two massively instrumented solute transport experiments were performed in desert soils near Las Cruces, New Mexico (Wierenga et al. 1991; Hills et al. 1991). Drip emitters were used to irrigate a plot adjoining a deep trench in a heterogeneous soil possessing well in excess of one order of magnitude standard deviation in saturated hydraulic conductivity. Monitoring of the trench face showed a spatially uniform progression of the wetting front and did not reveal indications of preferential flow (Wierenga et al. 1991). Hills et al. (1991) found that a dispersivity of 5 cm provided reasonably realistic simulations of ^3H and Br tracer distributions.

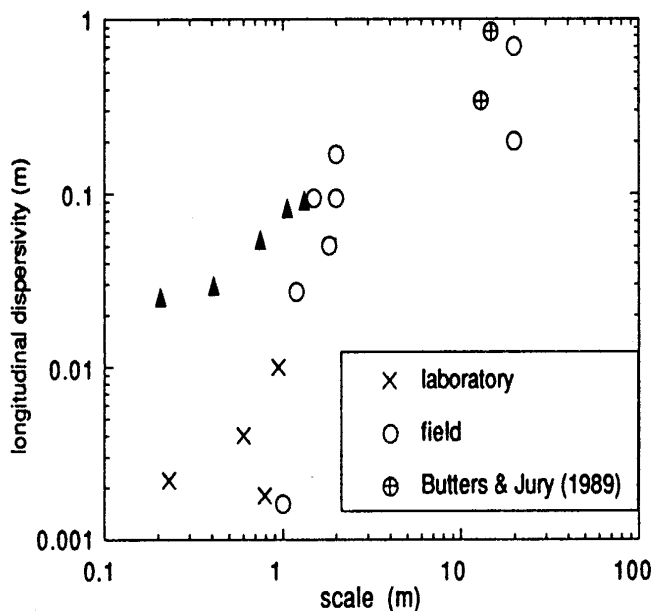


Figure 13. Longitudinal macrodispersivity in unsaturated media as a function of overall problem scale (after Gelhar 1993). [Note that the triangles are data from Ward et al. 1998]

For unsaturated flow, long-term environmental tracer studies at several arid southwestern sites indicate dispersivities of less than 10 cm. Phillips et al. (1988) assessed the degree of mixing in desert soils using the conventional advection-dispersion modeling, yielding

a dispersion coefficient of 50 cm²/yr. This compares with the calculated effective diffusion coefficient of 25 cm²/yr. A similar study by Scanlon (1992), at another southwestern arid site, obtained a dispersion coefficient of about 14 cm²/yr. These, then, lead to effective dispersivities of about 7 and 4 cm, at the two arid sites, and Peclet numbers (displacement divided by dispersivity) of 23 and 17.

Ward et al. (1998)³ obtained dispersivity estimates via field measurements at a location close to the ILAW site, using KCl as a tracer. Analysis of the data provided dispersivities that ranged from 1.3 to 7.8 cm for travel distances ranging from 25 to 125 cm (Appendix C). Dispersivity increased with depth to about 0.75 m, after which it essentially became constant. Although these estimates are for the Hanford formation similar to the ILAW site, the transport distance within the vadose zone is indeed of limited extent. Nevertheless, results based on the limited data are consistent with the concept of a scale-dependent dispersivity. Thus, although no data exist on large-scale dispersivities near the ILAW site, it is expected that they will be larger than those based on the small-scale tracer experiment of Ward et al. (1998).

Based on a survey of literature, Gelhar (1993) presented, as shown in Figure 13, the longitudinal vadose zone dispersivities as a function of the scale of the experiment. The figure shows a lack of data for scales larger than 2 m. Nevertheless, similar to saturated flow, Figure 13 show an increase of dispersivity with an increase in scale. Also, shown in Figure 13 are results from the Ward et al. experiment; their data are in close agreement with others.

3.2.3.3 Stochastic Models and Macrodispersivities for Large-Scale Media

Field-scale dispersivities are referred to as macrodispersivities. The heterogeneities that exist at various length scales result in a scale dependence of macrodispersivities. Stochastic models have been developed which relate the macrodispersive spreading to the spatial variability of saturated hydraulic conductivity field in a saturated porous media (e.g., Gelhar and Axness 1983; Dagan 1984). The Gelhar and Axness (1983) model provides the asymptotic estimates of macrodispersivity, while the Dagan (1984) model describes the preasymptotic estimates of macrodispersivities for the near-source, early-time period. The Dagan (1984) model predicts that under steady state flow with a uniform mean hydraulic gradient, the ensemble longitudinal macrodispersivity increases with time and displacement distance as the solute first enters the flow domain. A constant, asymptotic value (i.e., Fickian behavior) is eventually reached after the solute travels a few tens of correlation scales of the hydraulic conductivity field.

For prediction of contaminant transport during early time or for short travel distances, simulating effects of scale-dependence on macrodispersion is a consideration. The dispersivities increase with time (or equivalently with distance) until they tend to

³ Ward, A.L., R.E. Clayton, and J.S. Ritter. 1998. Determination of in situ hydraulic parameters of the upper Hanford formation. Letter Report to Fluor Daniel Northwest, Inc. December, 1998. Pacific Northwest National Laboratory. Richland, WA.

converge on their unique asymptotic (large time) values. The second-moment evolution curve or the time-dependent, preasymptotic macrodispersivities are of particular interest, since it can take a long time (e.g., years or decades) for the asymptotic Fickian approximation to take hold. However, the early time scale dependence are of little consequence in simulations involving long times or large mean travel distances such as those for ILAW PA. For these predictions over large travel distances or large times, the use of a constant (asymptotic) dispersivity is considered to be adequate. An estimate of the maximum or asymptotic value of macrodispersivity for saturated media can be based on Gelhar and Axness' (1983) stochastic solution:

$$A_L = \sigma_{LnKs}^2 \lambda \quad (5)$$

where λ is the vertical correlation scale (i.e., average distance over which conductivities are correlated) for log saturated hydraulic conductivity.

In addition to the size of flow domain and vadose zone soil heterogeneities, dispersivities are expected to be a function of soil moisture content (or matric potential). Macrodispersivities are expected to increase with a decrease in saturation (e.g., Polmann 1990; Gelhar et al. 1994). Russo (1993) suggests that vadose zone macrodispersivities can be defined in a manner similar to saturated media estimates. This is based on his finding that the product of the variance and the correlation scale of log conductivity for both saturated and unsaturated media are of similar magnitude. In other words, an increase in the variance of log conductivity (and, concurrently, in the velocity variance) as moisture content decreases is compensated in part by a decrease in the correlation scale of log conductivity (and, concurrently, in the correlation scale of the longitudinal component of the velocity). Such an approximation (a) assumes use of Gardner's (1958) equation to describe unsaturated conductivity as a function of matric potential, and (b) holds as long as the correlation scale of λ in Gardner's equation is relatively small compared with that of log saturated conductivity.

3.2.3.4 Macrodispersivity Estimates For Non-Reactive Species

The Gelhar and Axness equation can be used to estimate asymptotic values of macrodispersivity. However, to account for effects of unsaturated flow, a modified version is used for both disposal sites:

$$A_L(\langle \psi \rangle) = \sigma_{LnK}^2 \lambda \quad (6)$$

where the longitudinal macrodispersivity depends on the mean tension $\langle \psi \rangle$. To apply equation (6), an estimate of the vertical correlation scale for unsaturated conductivity is needed. As discussed earlier, a correlation length of the order of about 50 cm was obtained for the sandy formation. However, compared to the saturated K's, an increase in the variance of log conductivity is expected to be compensated in part by a decrease in the correlation scale of log unsaturated conductivity. A correlation length of 30 cm is assumed for both sandy and gravelly formations. Table 6 provides the log unsaturated

conductivity variances (at a recharge rate of about 0.1 cm/yr) and the estimated longitudinal (A_L) and transverse (A_T) macrodispersivities for the two formations. The transverse dispersivities are estimated as $1/10^{\text{th}}$ of the longitudinal values (Gelhar et al. 1992). Gelhar (1993) presented results of stochastic analysis of macrodispersion in unsaturated media by Mantoglou and Gelhar (1985). The large-scale macrodispersivity estimates in Table 7 are of similar magnitude to those reported in Gelhar (1993) for Panoche and Maddock soil types.

Table 7. Non-reactive macrodispersivity estimates for soils at the new ILAW and existing disposal sites.

Formation	σ_{LnK}^2	Correlation length, • (cm)	A_L (cm)	A_T (cm)
Sandy	5.51	30	~200	20
Gravelly	0.96	30	~30	3

3.2.3.5 Heterogeneous Sorption Enhanced Macrodispersivities

As expected, the net effect of sorption is to retard the velocity of the contaminant in the soil. Because sorption for specific contaminants may be a function of soil properties, as the soil properties experience spatial variability, the sorption also varies (Gelhar 1993; Talbott and Gelhar 1994). The variation directly affects the velocity of the contaminant, which, in turn, enhances the spreading of the plume. The enhanced spreading is defined by a larger reactive longitudinal macrodispersivity, different from the non-reactive longitudinal macrodispersivity, as discussed in the preceding section. The increased plume spreading due to heterogeneous sorption (over and above the result for no sorption) is defined as the macrodispersivity enhancement. Stochastic theory and field data on contaminant plumes suggest that the effect of macrodispersivity enhancement only occurs in the longitudinal direction. The transverse macrodispersivity is unaffected by sorption variability (Garabedian et al. 1991). The results presented in this section will support the use of species-dependent enhanced longitudinal macrodispersivities in the ILAW PA modeling.

The radioisotopes considered are Cs-137, Sr-90, U, and Se. The objective is to evaluate differences in macrodispersivity enhancement due to a long-lived mobile radionuclide (e.g., U) and a short-lived relatively immobile radionuclide (e.g., Sr-90). During the laboratory analysis, measurements of K_d for each species have been obtained on the same soil samples, as are measurements of unsaturated hydraulic conductivity.

Based on laboratory measurements of unsaturated conductivity, K (Fayer et al. 1998; see footnote on p. 4) and K_d (Kaplan et al. 1998) for the same 20 samples for the Hanford

sandy sequence, a direct correlation of K and K_d was derived for Cs-137, Sr-90, U, and Se. Stochastic theory developed by Gelhar (1993) was evaluated to determine the importance of varying longitudinal macrodispersivity by contaminant species on the basis of sorption heterogeneity and correlation with hydraulic conductivity. An enhancement of macrodispersivity can have significant effects on the expected contaminant predictions for numerical models.

In order to understand clearly the importance of heterogeneous, spatially variable sorption, a number of parameters were defined. The variable K_d may be prescribed by a mean (\bar{K}_d) and a standard deviation (σ_{K_d}). Further, a retardation factor, R , was related to K_d by the following:

$$R = 1 + \frac{\rho_b K_d}{\theta} \quad (7)$$

where R may be described statistically by an effective retardation, $\bar{R} = E[R]$, and its standard deviation, σ_R .

By analyzing the mean and standard deviation of a sample data set of a measured soil property, and by showing a relationship between the soil property and R , \bar{R} and σ_R were calculated as a function of the soil property data set.

The net result of the variation in the retardation and the relationship between the retardation and σ_{LnK} is to increase the longitudinal macrodispersivity of the sorbed species according to the following equation given by Talbott and Gelhar (1994):

$$A_{11} = A_0 \left\{ \left[1 + \gamma \frac{\sigma_R}{R \sigma_{LnK}} \sqrt{\zeta} \right]^2 + (1 - \zeta) \frac{\sigma_R^2 \lambda_n}{\bar{R}^2 \sigma_{LnK}^2 \lambda_1} \gamma^2 \right\} \quad (8)$$

where A_0 is the non-reactive longitudinal macrodispersivity, σ_1 is the horizontal correlation scale, σ_n , σ_1 , and σ is defined as the ratio of harmonic to geometric mean for unsaturated K .

Equation (8) is identical to that in Talbott and Gelhar (1994), except that the appropriate variables are evaluated for unsaturated conditions. Equation (8) assumes random K_d but constant bulk density and moisture content. However, using the more general case (p. 256, Gelhar 1993) when all three (i.e., K_d , bulk density and moisture content) vary, it was found that the contribution to equation (8) from variations of bulk density and moisture content were negligibly small, compared to variations of K_d .

The LnK versus R relation for the four species for the sandy sequence are shown in Figure 14. The result of stochastic analysis for macrodispersivity enhancement for the Hanford sandy sequence is shown in Table 8. Note that the unsaturated K 's were

evaluated at -100 cm via the fitted van Genuchten-Mualem relation. As expected, the log conductivity variance, σ_{LnK}^2 at a matric potential of -100 cm is much higher (~5.5) compared to the σ_{LnKs}^2 (~1.0) for the same 20 samples at saturation. The macrodispersivity enhancement, A_{11}/A_0 ranges from about 1.06 for Se to about 2.12 for U.

Table 8. Macrodispersivity enhancement for the sandy sequence at the new ILAW and existing disposal sites [ρ_b in g/cm³ and K_d in cm³/g].

Species	$\overline{K_d}$	$\sigma_{K_d}/\overline{K_d}$	\overline{R}	σ_R/\overline{R}	$\overline{\rho_b}$	$\overline{\theta}$	σ_{LnK}^2	σ_{LnK}	σ_{LnK}	σ_{LnK}	A_{11}/A_0
Cs-137	2055	0.29	31002	0.50	1.71	0.138	5.51	0.22	0.52	1	1.07
Sr-90	14.7	0.11	241	0.62	1.71	0.138	5.51	0.22	0.45	1	1.08
U	0.62	0.20	11.1	0.52	1.71	0.138	5.51	0.22	0.53	1	2.12
Se	6.73	0.28	98.5	0.28	1.71	0.138	5.51	0.22	0.68	1	1.06

The LnK versus R relation for the four species for the gravelly sequence are shown in Figure 15. The result of stochastic analysis for macrodispersivity enhancement for the Hanford gravelly sequence is shown in Table 9. Again, the unsaturated K's were evaluated at -100 cm via the fitted van Genuchten-Mualem relation for the 15 gravelly samples. No data are available on the measurements of sorption coefficients for the gravel-dominated sequence. Based on the information for the sandy samples, all gravelly samples were first assigned the same average sorption coefficient for their respective species. This resulted in the coefficient of variation (i.e., Col. 3 in Table 9) to be identically zero for all four species. The bulk (gravel and fine fraction) retardation coefficients are then based on a correction of the actual surface area available for sorption, based on the individual gravel fraction for the 15 samples. Unlike for the sandy sequence, the log conductivity variance, σ_{LnK}^2 at a matric potential of -100 cm is much lower (~0.96) compared to the σ_{LnKs}^2 (~5.31) for the same 15 samples at saturation. The macrodispersivity enhancement, A_{11}/A_0 varies over a very narrow range -- from about 1.05 for U to about 1.07 for Cs-137.

Table 9. Macrodispersivity enhancement for the gravelly sequence at the new ILAW and existing disposal sites [ρ_b in g/cm³ and K_d in cm³/g].

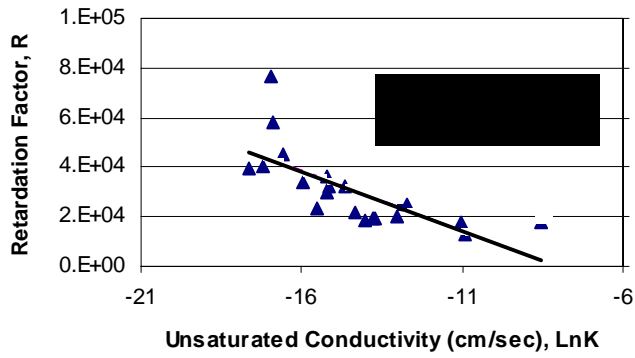
Species	\bar{K}_d	σ_{K_d}/\bar{K}_d	\bar{R}	σ_R/\bar{R}	$\bar{\rho}_b$	$\bar{\theta}$	$\sigma_{\ln K}^2$	σ	σ	$\sigma_{n/1}$	A_{11}/A_0
Cs-137	2055	0	17148	0.21	2.19	0.10	0.96	0.62	0.033	1	1.07
Sr-90	14.7	0	124	0.20	2.19	0.10	0.96	0.62	0.033	1	1.06
U	0.62	0	6.13	0.17	2.19	0.10	0.96	0.62	0.033	1	1.05
Se	6.73	0	57.12	0.20	2.19	0.10	0.96	0.62	0.033	1	1.06

3.2.3.6 Numerical Considerations

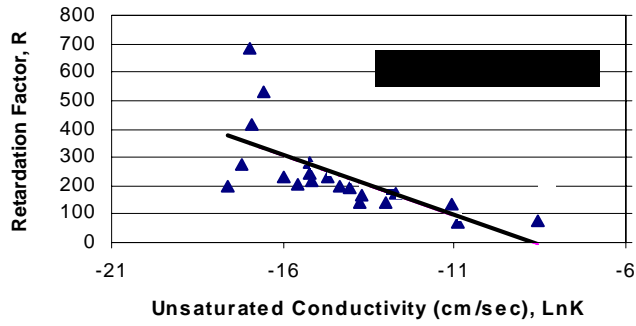
A complicating factor in numerical modeling of contaminant transport in porous media is that both finite-difference and finite-element solutions are affected by "numerical dispersion," which refers to artificial dispersion caused by errors associated with discretization of the flow domain. To minimize such errors, the grid should be designed so that the Peclet number ($P_e = \text{discretized distance}/\text{dispersivity}$) is less than or equal to one, although acceptable solutions can be obtained with P_e as high as 10 (Huyakorn and Pinder 1983). With low dispersivities within the vadose zone, the Peclet number criterion results in grid spacings that are not very practical to implement. This is why numerical modelers often resort to higher values of dispersivity. An alternative is to consider use of "upwinding" option (Huyakorn and Pinder 1983) to control numerical dispersion.

Another consideration is discretization of simulation time so that the Courant number ($C_r = \text{pore velocity} \times \text{time interval}/\text{grid spacing}$) is less than or equal to one. That is, the time step should be selected so that the chosen time interval is less than the value obtained by the ratio of grid spacing to pore velocity. Thus, the time step should be selected so that it is less than the time it takes for the solute to move one grid spacing. Note that, for a three-dimensional problem, the P_e and C_r criteria are applicable to transport in all three directions.

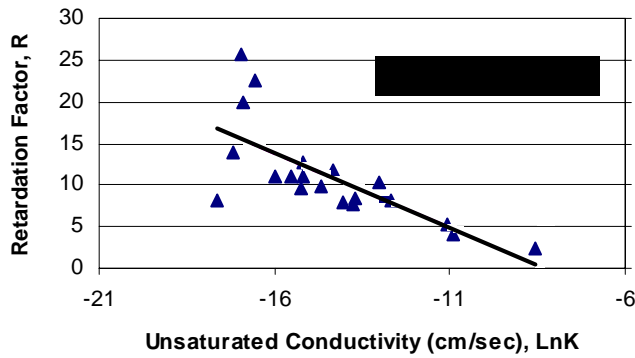
(a)



(b)



(c)



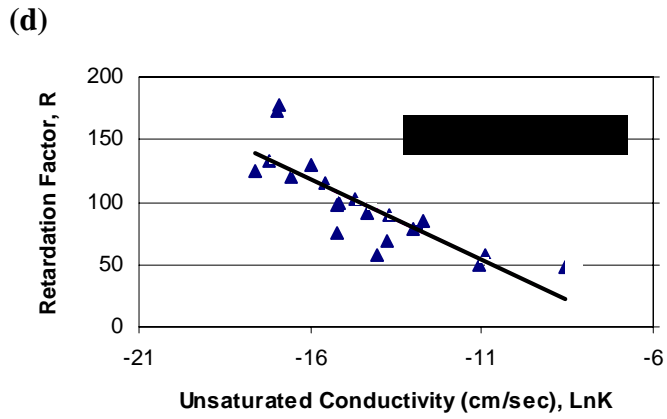
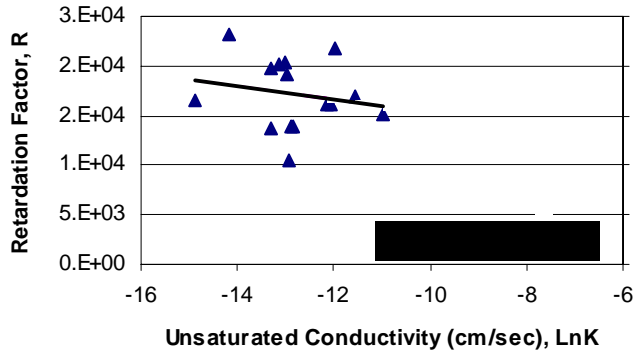
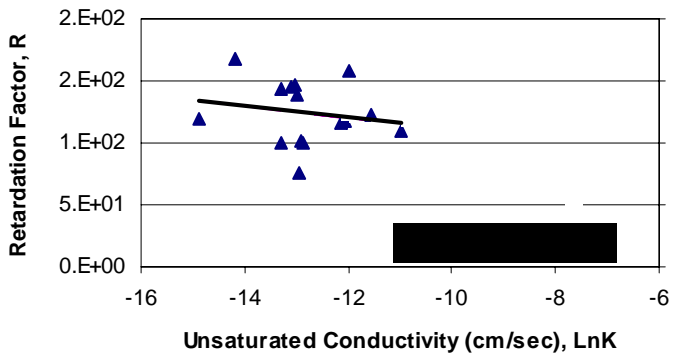


Figure 14. LnK versus R for (a) Cs-137, (b) Sr-90, (c) U, and (d) Se for the sand-dominated sequence.

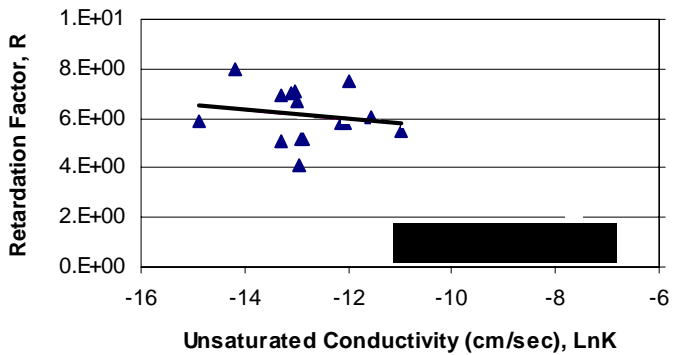
(a)



(b)



(c)



(d)

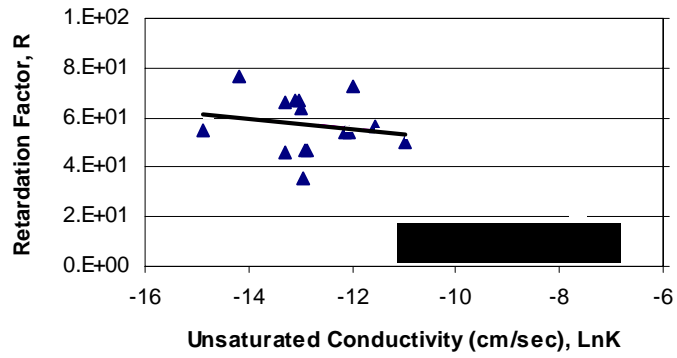


Figure 15. LnK versus R for (a) Cs-137, (b) Sr-90, (c) U, and (d) Se for the gravel-dominated sequence.

4.0 UNCERTAINTIES IN MODEL PREDICTIONS

As discussed in the preceding sections, the application of stochastic theory resulted in effective (upscaled) parameter estimates for saturated hydraulic conductivity, soil moisture retention and unsaturated hydraulic conductivity, bulk density, unretarded macrodispersivity and sorption-enhanced macrodispersivity. These parameters will serve as input to VAM3DF (Huyakorn and Panday 1995), a variably saturated flow and transport code; VAM3DF will generate 'mean' solutions for the pressure head and contaminant concentration.

The breakthrough curve due to contaminants released from the disposal facility is expected to appear as a "step" function at the water table, with the shape of the rise of the step function primarily governed by vadose zone heterogeneity, macrodispersivity, sorption, and radionuclide decay. Because of the long release time for the contaminants from the disposal facility, compared to the travel time through the vadose zone, it is reasonable to approximate the contaminant release as a step input function.

Three sources contribute to uncertainty calculations: (a) variations in model configurations, (b) uncertainties *in* the calculated mean concentration distribution at the water table, and (c) uncertainties *around* the calculated mean concentration distribution at the water table. Figure 16 illustrates the expected concentration distribution at the water table. The sigmoid-shaped mean concentration distribution (Figure 16) is calculated by VAM3DF, based on a particular conceptual model configuration and sensitivities to effective input parameters. However, the mean solution should be viewed as being an average of many 'realizations.' In other words, the expected peak concentration is not necessarily the calculated mean concentration (Figure 16). There is variation among different realizations, because of vadose zone heterogeneities. The variance (σ_c^2) about the mean characterizes such variation *around* a particular mean solution. While the uncertainties *in* the mean solution are calculated directly by VAM3DF, uncertainties *around* the calculated mean solution will be estimated based on available stochastic solutions, as described later.

4.1 Model Configurations

4.1.1 Variations in Stratigraphy

At this time, a basic layered geologic model is being postulated for VAM3DF base case calculations. Such a model is based on the most recent geologic information (Reidel et al. 1998; Kincaid et al. 1995) available on the stratigraphy at the two sites. Dips and inclines (as identified in the geology data package) of the various strata will be considered as part of variations of base case model configurations for both disposal sites. Such variations of the basic stratigraphic cross-sections at the two sites are part of the geology data package.

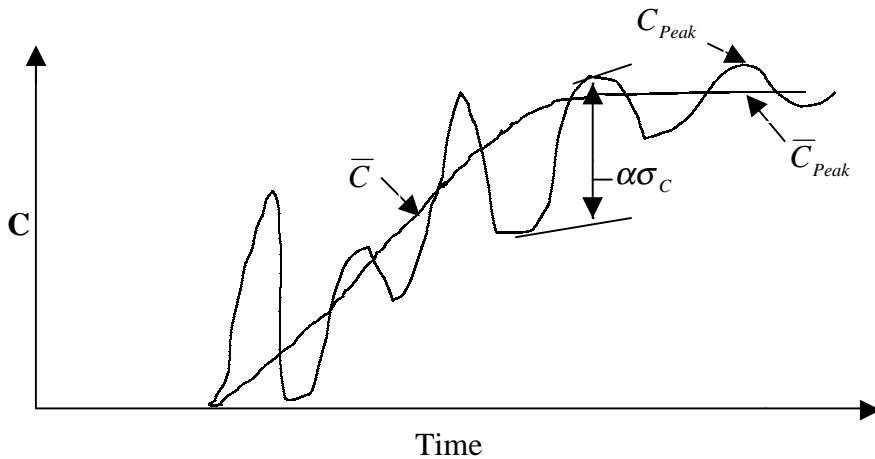


Figure 16. Schematic of concentration (C) distribution at the water table.

[\bar{C} = calculated mean concentration, \bar{C}_{Peak} = calculated mean peak concentration, C_{Peak} = peak concentration, σ_C = standard deviation of variation around the calculated mean solution, $\alpha\sigma_C$ = multiple of variation around the calculated mean solution for a particular model configuration and input effective parameters.]

4.1.2 Clastic dikes

Clastic dikes are ubiquitous sedimentary structures observed in outcrops and trenches that expose the Hanford formation in the 200 Areas. Their distribution, orientation, and other important characteristics are provided as part of the geology data package. The dikes are believed to represent dewatering structures that developed during compaction and settling of cataclysmic flood deposits during or soon after floodwaters drained from the Pasco Basin. The true nature and extent of clastic dikes are difficult to determine, because the dikes are rarely detected or observed in vertically oriented boreholes. Often they form a polygonal pattern where they intersect the ground surface.

An extensive atlas developed by Fecht et al. (1999)⁴ addresses a subset of dikes (i.e., clastic injection dikes) that have been formed as a result of sediments in fissures. Clastic injection dikes are fissures which may total a meter or more in thickness. These dikes are typically filled with poor to well-sorted sand, but may also contain silt, clay, and gravel.

⁴ Fecht, K.R., K.A. Lindsey, B.N. Bjornstad, D.G. Horton, G.V. Last, and S.P. Reidel. 1999. Clastic Injection Dikes of the Pasco Basin and Vicinity. BHI-01103 Rev. 0. July, 1999. Bechtel Hanford Inc. Richland, WA.

These dikes are of particular interest to the ILAW PA because they occur as near-vertical tabular bodies filled with multiple layers of unconsolidated sediments. Thin clay/silt linings separate the margins of most dikes and internal layers within dikes.

It is important to develop an understanding of the potential presence of these discrete structures in the vicinity of disposal sites such that uncertainties in flow and transport calculations can be adequately accounted for. Such an understanding on the presence of clastic dike networks in the vicinity of disposal sites will be provided as part of the geology data package. The potential for clastic injection dikes to provide preferential pathways will be examined as part of variations of model configurations at both disposal sites.

One particular scenario will be considered to provide a bounding estimate: presence of a near-vertical (or otherwise as characterized in geology data package) clastic dike directly below a vault and extending through the Hanford formation (or as identified in the geology data package). The width of the dike will be based on information in the geology data package.

Data on physical and hydraulic parameters are needed for clastic dike infilling materials to model their effects on flow and contaminant transport. Such physical and hydrologic properties (e.g., bulk density, particle-size distribution, moisture retention, saturated and unsaturated hydraulic conductivities) for clastic dike infilling materials are included in Fayer and Ritter (1999)⁵. A summary of the physical and hydraulic parameters is given in Table 10. As suggested in Table 10, the measured properties represent fine material. Other database (e.g., Fecht et al. 1998) will be consulted for possible presence of coarse infilling materials in a clastic dike.

Table 10. Van Genuchten parameters (based on the multistep method), saturated hydraulic conductivity, and bulk density for seven clastic dike samples (after Fayer and Ritter 1999).

Sample	θ_s (cm ³ /cm ³)	θ_r (cm ³ /cm ³)	α (1/cm)	n (-)	Saturated Hydraulic Conductivity (cm/s)	Bulk Density (g/cm ³)
1	0.424	0.063	0.0839	1.33	5.97E-04	1.57
2A	0.446	0.019	0.0762	1.98	4.70E-03	1.50
2B	0.443	0.023	0.0741	1.84	3.14E-03	1.51
3A	0.424	0.025	0.0143	2.49	3.41E-03	1.46
3B	0.448	0.050	0.0593	1.54	1.14E-03	1.52
4A	0.454	0.030	0.0092	1.97	1.84E-03	1.49
4B	0.425	0.021	0.0823	2.09	5.43E-03	1.57

⁵ Fayer M.J. and J.S. Ritter. 1999. Physical and hydraulic measurements of FY 1998 clastic dike samples. Letter Report to Fluor Daniel Northwest, Inc. March, 1999. Pacific Northwest National Laboratory. Richland, WA.

4.1.3 Isotropy

The base case simulations will consider a layer-cake stratigraphy and tension-dependent anisotropy. This is expected to result in more of lateral than vertical migration of contaminants. A variation of the base case will consider an isotropic case. This is expected to result in enhanced vertical migration, compared to the base case.

4.1.4 Sloped Layering

Another case that will be considered has to do with the combined effects of variation in stratigraphy and anisotropy. For unsaturated flow, the degree of anisotropy depends not only on the variability of soil hydraulic properties, but also on the orientation of the soil layers relative to the mean hydraulic gradient. The tension-dependent anisotropy relationships will be reevaluated for dips and inclines identified (in geology data package) for variations in base case stratigraphy, and their effects examined via VAM3DF simulations.

4.2 Uncertainties in the Mean Solution due to Variations of Effective Parameter Estimates

As mentioned earlier, uncertainties in the mean solution are due to variations in conceptual model configuration and sensitivities to effective input parameters. Variations in conceptual model configuration have been discussed in the preceding section. Sensitivities to effective input parameter variations are discussed in this section.

The sensitivity of the model predictions to uncertainties in the effective parameters will be considered for two important parameters, i.e., unsaturated conductivity and macrodispersivity. Sensitivity of these two effective parameters and their estimated effects on the mean solution are discussed below. Note that variations in saturated conductivity will not be considered, since the moisture regime within the far-field vadose zone for the disposal sites is not expected to be at or near saturation. It should also be noted that recharge and variations in recharge estimates are another source of uncertainty. However, sensitivities to recharge estimates will be propagated via changes in effective parameter estimates for unsaturated conductivity and macrodispersivity.

The stratigraphy at both disposal sites is dominated by two distinctly different sediment sequences. The upper part of the vadose zone is characterized by a sandy sequence, whereas the lower part is characterized primarily by a gravel sequence. At saturation, compared to the gravel-dominated sequence, the sand-dominated sequence is described by a smaller log-conductivity variance. However, compared to the gravel-dominated sequence, the log-unsaturated conductivity variance for the sand-dominated sequence is higher. The variations in unsaturated conductivities for both sandy and gravelly sequences are discussed in detail earlier. Variabilities in unsaturated conductivities lead to macroscopic anisotropy relations for the sandy and gravelly

sediments that are quite different. Consequently, VAM3DF simulations incorporating variations in macroscopic anisotropy relations will produce different mean concentration distributions at the water table.

A much more important parameter that will affect mean concentration distribution, for a given model configuration, is macrodispersivity. Typically, in modeling transport, the same unretarded dispersivity value is assumed for all transported (retarded and unretarded) species. VAM3DF simulations will consider, for the transported species, comparisons of enhanced longitudinal macrodispersivity with that of a nonretarded macrodispersivity. The variability in these estimates, along with professional judgement (e.g., an increase or decrease of 25% of estimated macrodispersivities), will be used to quantify uncertainties in the mean solution.

Note that each VAM3DF-calculated mean solution incorporates effects due to model configuration variations and sensitivities to effective input parameter variations. The goal will be to limit the number of VAM3DF runs. Nevertheless, once the mean solutions are obtained for various VAM3DF runs, they can be used to obtain variance estimates for the mean solutions, and therefore characterize the uncertainty in the mean solutions.

4.3 Uncertainties Around the Mean Solution

As described earlier, since the effective concentration predictions represent a mean solution, fluctuations about this mean, due to heterogeneity, are another source of uncertainty. The variations in concentrations around the mean concentration can be characterized through a stochastic evaluation of the concentration variance. It will be assumed that the developed theory for the nonretarded species is applicable to the case with spatially variable sorption, provided that the enhanced macrodispersivity is used for the sorbing species. The concentration variance tends to be large in regions close to the source where concentration gradients are large. Using stochastic approaches described by Kapoor and Gelhar (1994a,b), the coefficient of variation of concentration will be estimated at the water table. Detailed equations are presented in Kapoor and Gelhar, but briefly the concentration variance is directly proportional to the mean concentration gradient for the VAM3DF-calculated mean concentration distribution at the water table and the longitudinal macrodispersivity, and inversely proportional to the local dispersivity values.

4.4 Bounding Estimates

Note that the cumulative effect of uncertainties is not additive. Rather, bounding scenarios will be based on combinations of various worst case conditions. For example, a bounding scenario may be postulated as the one having isotropic material properties for both sand- and gravel-dominated sequences, high recharge, clastic dike, and minimum values of macrodispersivity. In other words, bounding estimates will be dictated by

selected model configuration and effective parameter estimates that produce a higher mean concentration at the water table.

5.0 REFERENCES

- Bacon, D. J. and B. P. McGrail. 1997. Source Term Analysis for Hanford Low-Activity Tank Waste Using the STORM Code: A Coupled Unsaturated Flow and Transport Model, in *Symposium on Science and Technology for Disposal of Radioactive Tank Wastes*, ed. N.J. Lombardo and W.W. Schulz. Plenum Publishing. Las Vegas, NV.
- Bear, J., C. Braester and P. C. Menier. 1987. Effective and relative permeabilities of anisotropic porous media. *Transport in Porous Media* 2: 301-316.
- Dagan, G. 1984. Solute transport in heterogeneous porous formations. *J. Fluid Mech.* 145:151-157.
- Eching S. O, and J. W. Hopmans. 1993. Optimization of hydraulic functions from transient outflow and soil water pressure data. *Soil Sci. Soc. Am. J.* 57:1167-1175.
- Freeze, R. A. and J. A. Cherry. 1979. *Groundwater*. Prentice-Hall, Inc., Englewood Cliffs, NJ.
- Garabedian, S. P., D. R. LeBlanc, L. W. Gelhar, and M. A. Celia, Large-scale Natural-gradient Tracer Test in Sand and Gravel, Cape Cod, Massachusetts: 2, Analysis of Tracer Moments for a Nonreactive Tracer, *Water Resources Research*, 27(5), 911-924, 1991.
- Gardner, W. H. 1986. Water Content, in *Methods of Soils Analysis, Part I*, edited by A. Klute, pp. 493-544. Amer. Soc. of Agron. Madison, Wisc.
- Gardner, W. R. 1958. Some steady-state solutions of the unsaturated moisture flow equation with applications to evaporation from a water table. *Soil Sci.* 85:228-232.
- Gelhar, L. W., M. A. Celia and D. McLaughlin. 1994. *Modeling Field Scale Unsaturated Flow and Transport Processes*. NUREG/CR-5965. Nuclear Regulatory Commission, Washington, D.C.
- Gelhar, L. W., C. Welty, and K. R. Rehfeldt. 1992. A critical review of data on field-scale dispersion in aquifers. *Water Resour. Res.* 28:1955-1974.
- Gelhar, L. W. 1993. *Stochastic Subsurface Hydrology*, Prentice Hall, New York.
- Gelhar, L. W. and C. L. Axness. 1983. Three-dimensional analysis of macrodispersion in a stratified aquifer. *Water Resour. Res.* 19:161-180.

- Green, T. R. and D. L. Freyberg. 1995. State-dependent anisotropy: comparisons of quasi-analytical solutions with stochastic results for steady gravity drainage. *Water Resour. Res.* 31:2201-2212.
- Hills, R. G., P. J. Wierenga, D. B. Hudson, and M. R. Kirkland. 1991. The second Las Cruces Trench experiment: experimental results and two-dimensional flow predictions. *Water Resour. Res.* 27:2707-2718.
- Huyakorn, P. S. and S. Panday. 1995. VAM3DF - A Variably Saturated Analysis Model in Three Dimensions for the Data Fusion System. HydroGeoLogic, Inc. Herndon, VA.
- Huyakorn, P. S. and G. F. Pinder. 1983. *Computational Methods in Subsurface Flow*. Academic Press, NY.
- Kaplan, D. I., K. E. Parker and I. V. Kutynakov. 1998. Radionuclide Distribution Coefficients for Sediments Collected from Borehole 299-E17-21: Final Report for Subtask 1a. PNNL-11966. Pacific Northwest National Laboratory. Richland, WA.
- Kapoor, V. and L. W. Gelhar. 1994a. Transport in three-dimensionally heterogeneous aquifers 1. Dynamics of concentration fluctuations. *Water Resour. Res.* 30:1775-1788.
- Kapoor, V. and L. W. Gelhar. 1994b. Transport in three-dimensionally heterogeneous aquifers 2. Predictions and observations of concentration fluctuations. *Water Resour. Res.* 30:1789-1801.
- Khaleel, R. and J. F. Relyea. 1997. Correcting laboratory-measured moisture retention data for gravels. *Water Resour. Res.* 33:1875-1878.
- Khaleel, R., J. F. Relyea and J. L. Conca. 1995. Evaluation of van Genuchten-Mualem relationships to estimate unsaturated conductivity at low water contents. *Water Resour. Res.* 31:2659-2668.
- Khaleel, R. and E. J. Freeman. 1995a. *Variability and Scaling of Hydraulic Properties for 200 Area Soils, Hanford Site*. WHC-EP-0883. Westinghouse Hanford Company. Richland, Washington.
- Khaleel, R. and E. J. Freeman. 1995b. *A Compilation of Hydrologic Properties for Low-Level Tank Waste Disposal Facility Performance Assessment*. WHC-SD-WM-RPT-165, Rev. 0. Westinghouse Hanford Company. Richland, Washington.
- Kincaid, C. T., J. W. Shade, G. A. Whyatt, M. G. Piepho, K. Rhoads, J. A. Voogd, J. H. Westsik, Jr., M. D. Freshley, K. A. Blanchard, B. G. Lauzon. 1995. Performance

Assessment of Grouted Double-Shell Tank Waste Disposal at Hanford, WHC-SD-WM-EE-004, Rev. 1, Westinghouse Hanford Company. Richland, WA.

- Klute, A. 1986. Water Retention: Laboratory Methods, in *Methods of Soils Analysis, Part I*, edited by A. Klute, pp. 635-660. Amer. Soc. of Agron. Madison, Wisc.
- Klute, A. and C. Dirksen. 1986. Hydraulic Conductivity and Diffusivity: Laboratory methods, in *Methods of Soils Analysis, Part I*, edited by A. Klute, pp. 687-734. Amer. Soc. of Agron. Madison, WI.
- Kool, J. B., J. C. Parker, and M. T. van Genuchten. 1985a. Determining soil hydraulic properties from one-step outflow experiments by parameter estimation, I, Theory and numerical studies. *Soil Sci. Soc. Am. J.* 49:1348-1354.
- Kool, J. B., J. C. Parker, and M. T. van Genuchten. 1985b. Determining soil hydraulic properties from one-step outflow experiments by parameter estimation, II, Experimental studies. *Soil Sci. Soc. Am. J.* 49:1354-1359.
- Mann, F. M., R. P. Puigh, II, P.D. Rittmann, N. W. Kline, J. A. Voogd, , Y. Chen, C. R. Eiholzer, C. T. Kincaid, B. P. McGrail, A. H. Lu, G. F. Williamson, N. R. Brown and P. E. LaMont. 1998. *Hanford Immobilized Low-Activity Tank Waste Performance Assessment*. DOE/RL-97-69, Rev.0, U.S. Department of Energy, Richland, WA.
- Mantoglou, A. and L. W. Gelhar. 1987. Stochastic modeling of large-scale transient unsaturated flow. *Water Resour. Res.* 23:37-46.
- Mantoglou, A. and L. W. Gelhar. 1985. Large scale models of transient unsaturated flow and contaminant transport using stochastic methods. Ralph M. Parsons Laboratory Tech. Rpt. 299. Massachusetts Institute of Technology. Cambridge, MA.
- McCord, J. T., D. B. Stephens and J. L. Wilson. 1991. Hysteresis and state-dependent anisotropy in modelling unsaturated hillslope hydrologic processes. *Water Resour. Res.* 27:1501-1518.
- McGrail, B. P., W.L. Ebert, D.H. Bacon, and D. M. Strachan. 1998. A Strategy to Conduct an Analysis of the long-term Performance of Low-Activity Waste Glass in a Shallow Subsurface Disposal System at Hanford. PNNL-11834. Pacific Northwest National Laboratory. Richland, WA.
- Millington, R. J. and J. P. Quirk. 1961. Permeability of Porous Solids. *Trans. Faraday Soc.* 57:1200-1207.
- Mualem, Y. 1984. Anisotropy of unsaturated soils. *Soil Sci. Soc. Am. J.* 48:505-509.

- Mualem, Y. 1976. A new model for predicting the hydraulic conductivity of unsaturated porous media. *Water Resour. Res.* 12:513-522.
- Phillips, F., J. Mattick, T. Duval, D. Elmore, and P. Kubik. 1988. Chlorine 36 and tritium from nuclear weapons fallout as tracers for long-term liquid and vapor movement in desert soils. *Water Resour. Res.* 24:1877-1891.
- Polmann, D. J. 1990. Application of Stochastic Methods to Transient Flow and Transport in Heterogeneous Unsaturated Soils. Ph.D. Thesis. Massachusetts Institute of Technology. Cambridge, MA.
- Reidel, S. P. and D. G. Horton. 1999. Geologic Data Package for 2001 Immobilized Low-Activity Waste Performance Assessment. PNNL-12257, Rev. 1. Pacific Northwest National Laboratory. Richland, WA.
- Reidel, S. P., K. D. Reynolds and D. G. Horton. 1998. Immobilized Low-Activity Waste Borehole 299-E17-21. PNNL-11957. Pacific Northwest National Laboratory. Richland, WA.
- Russo, D. 1993. Stochastic modeling of macrodispersion for solute transport in a heterogeneous unsaturated porous formation. *Water Resour. Res.* 29:383-397.
- Scanlon, B. R. 1992. Evaluation of liquid and vapor water flow in desert soils based on chlorine 36 and tritium tracers and nonisothermal flow simulations. *Water Resour. Res.* 28:285-297.
- Sisson, J. B. and A. H. Lu. 1984. *Field Calibration of Computer Models for Application to Buried Liquid Discharges: A Status Report.* RHO-ST-46P. Rockwell Hanford Operations, Richland, WA.
- Stephens, D. B. and S. Heermann. 1988. Dependence of anisotropy on saturation in a stratified sand. *Water Resour. Res.* 24:770-778.
- Talbott, M. E. and L. W. Gelhar, *Performance Assessment of a Hypothetical Low-Level Waste Facility: Groundwater Flow and Transport Simulation*, NUREG/CR-6114 Vol. 3, U.S. Nuclear Regulatory Commission, Washington, D.C., 1994.
- van Genuchten, M. Th. 1980. A closed-form solution for predicting the conductivity of unsaturated soils. *Soil Sci. Soc. Am. J.* 44:892-898.
- van Genuchten, M. Th., F. J. Leij, and S. R. Yates. 1991. *The RETC code for quantifying the hydraulic functions of unsaturated soils.* U.S. E.P.A., EPA/600/2-91/065.
- Wierenga, P. J., R. G. Hills, and D. B. Hudson. 1991. The Las Cruces Trench site: Characterization, experimental results, and one-dimensional flow predictions. *Water Resour. Res.* 27:2695-2706.

- Yeh, T.-C. J. and D. J. Harvey. 1990. Effective unsaturated hydraulic conductivity of layered sands. *Water Resour. Res.* 26:1271-1279.
- Yeh, T.-C. J., L. W. Gelhar and A. L. Gutjahr. 1985a. Stochastic analysis of unsaturated flow in heterogeneous soils, 1. statistically isotropic media. *Water Resour. Res.* 21:447-456.
- Yeh, T.-C. J., L. W. Gelhar and A. L. Gutjahr. 1985b. Stochastic analysis of unsaturated flow in heterogeneous soils, 2. statistically anisotropic media with variable • . *Water Resour. Res.* 21:457-464.
- Yeh, T.-C. J., L. W. Gelhar and A. L. Gutjahr. 1985c. Stochastic analysis of unsaturated flow in heterogeneous media, 3. observations and applications. *Water Resour. Res.* 21:465-471.

6.0 PEER REVIEW

Practice 134 290 1112
 Publication Date 22Nov99
 Attachment 02 - Sheet 1 of 1

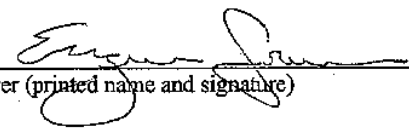
FLUOR DANIEL NORTHWEST

TECHNICAL PEER REVIEWS

CHECKLIST FOR TECHNICAL PEER REVIEW

Document Reviewed: FAR-FIELD HYDROLOGY DATA PACKAGE FOR IMMOBILIZED
 Title: LOW-ACTIVITY TANK WASTE PERFORMANCE ASSESSMENT
 Author: RAZ KHALEEL
 Date: DECEMBER 3, 1999
 Scope of Review:

Yes	No*	NA	
<input checked="" type="checkbox"/>	<input type="checkbox"/>	<input type="checkbox"/>	** Previous reviews complete and cover analysis, up to scope of this review, with no gaps.
<input checked="" type="checkbox"/>	<input type="checkbox"/>	<input type="checkbox"/>	Problem completely defined.
<input type="checkbox"/>	<input type="checkbox"/>	<input checked="" type="checkbox"/>	Accident scenarios developed in a clear and logical manner.
<input checked="" type="checkbox"/>	<input type="checkbox"/>	<input type="checkbox"/>	Necessary assumptions explicitly stated and supported.
<input checked="" type="checkbox"/>	<input type="checkbox"/>	<input type="checkbox"/>	Computer codes and data files documented.
<input checked="" type="checkbox"/>	<input type="checkbox"/>	<input type="checkbox"/>	Data used in calculations explicitly stated in document.
<input checked="" type="checkbox"/>	<input type="checkbox"/>	<input type="checkbox"/>	Data checked for consistency with original source information as applicable.
<input checked="" type="checkbox"/>	<input type="checkbox"/>	<input type="checkbox"/>	Mathematical derivations checked including dimensional consistency of results.
<input checked="" type="checkbox"/>	<input type="checkbox"/>	<input type="checkbox"/>	Models appropriate and used within range of validity, or use outside range of established validity justified.
<input checked="" type="checkbox"/>	<input type="checkbox"/>	<input type="checkbox"/>	Hand calculations checked for errors. Spreadsheet results should be treated exactly the same as hand calculations.
<input checked="" type="checkbox"/>	<input type="checkbox"/>	<input type="checkbox"/>	Software input correct and consistent with document reviewed.
<input checked="" type="checkbox"/>	<input type="checkbox"/>	<input type="checkbox"/>	Software output consistent with input and with results reported in document reviewed.
<input checked="" type="checkbox"/>	<input type="checkbox"/>	<input type="checkbox"/>	Limits/criteria/guidelines applied to analysis results are appropriate and referenced.
<input type="checkbox"/>	<input type="checkbox"/>	<input checked="" type="checkbox"/>	Limits/criteria/guidelines checked against references.
<input type="checkbox"/>	<input type="checkbox"/>	<input checked="" type="checkbox"/>	Safety margins consistent with good engineering practices.
<input checked="" type="checkbox"/>	<input type="checkbox"/>	<input type="checkbox"/>	Conclusions consistent with analytical results and applicable limits.
<input checked="" type="checkbox"/>	<input type="checkbox"/>	<input type="checkbox"/>	Results and conclusions address all points required in the problem statement.
<input type="checkbox"/>	<input type="checkbox"/>	<input checked="" type="checkbox"/>	Format consistent with applicable guides or other standards.
<input type="checkbox"/>	<input type="checkbox"/>	<input checked="" type="checkbox"/>	** Review calculations, comments, and/or notes are attached.
<input checked="" type="checkbox"/>	<input type="checkbox"/>	<input type="checkbox"/>	Document approved (for example, the reviewer affirms the technical accuracy of the document).

Eugene Freeman  December 3, 1999
 Reviewer (printed name and signature) Date

* All "no" responses must be explained below or on an additional sheet.
 ** Any calculations, comments, or notes generated as part of this review should be signed, dated, and attached to this checklist. The material should be labeled and recorded in such a manner as to be intelligible to a technically qualified third party.